

NNLO vertex corrections to non-leptonic B decays: Tree amplitudes

M. BENEKE, T. HUBER* and XIN-QIANG LI†

*Institut für Theoretische Physik E, RWTH Aachen University
D-52056 Aachen, Germany*

Abstract

The colour-suppressed tree amplitude in non-leptonic B decays is particularly sensitive to perturbative and non-perturbative corrections. We calculate the two-loop (NNLO) vertex corrections to the colour-suppressed and colour-allowed tree amplitudes in QCD factorization. Our results are given completely analytically, including the full dependence on the charm quark mass. We then update theoretical predictions for a range of interesting observables derived from $\pi\pi$, $\pi\rho$ and $\rho\rho$ final states that do not depend (significantly) on penguin contributions, and hence are now available with NNLO accuracy. We observe good agreement with experimental data within experimental and theoretical errors, except for observables involving the $\pi^0\pi^0$ branching fraction.

* Address after September 30, 2009: Fachbereich 7, Universität Siegen, Walter-Flex-Str. 3, 57068 Siegen, Germany

†Alexander-von-Humboldt Fellow

1 Introduction

Non-leptonic B decays are among the primary observables at the B factories. Their sheer number of more than a hundred final states offers a large number of observables: branching ratios, CP asymmetries, polarizations, as well as certain well-motivated combinations thereof. The large dataset accumulated by the B factories and the Fermilab Tevatron therefore allows for a rich phenomenology and for precise determinations of CKM and unitarity triangle parameters. In the future LHCb and a possible SuperB factory will further increase the amount of data; and they have the potential to discover yet unobserved channels and allow for an even more precise determination of quark flavour parameters.

Despite the fact that non-leptonic B decays are theoretically not as clean as for instance rare or radiative B decays, the amount of available experimental data justifies the need for precise theoretical predictions. A successful attempt to gain control over the complicated QCD effects in non-leptonic B decays is QCD factorization (QCDF) [1–4]. Within this approach hadronic matrix elements are represented as convolutions of perturbative objects (hard-scattering kernels) with non-perturbative quantities (light-cone distribution amplitudes, LCDA). It therefore constitutes a framework that systematically disentangles perturbative from non-perturbative physics. The factorization formula, valid at leading order in Λ_{QCD}/m_b and to all orders in α_s , reads

$$\begin{aligned} \langle M_1 M_2 | Q_i | \bar{B} \rangle = im_B^2 \left\{ f_+^{BM_1}(0) \int_0^1 du T_i^I(u) f_{M_2} \phi_{M_2}(u) \right. \\ \left. + \int_0^\infty d\omega \int_0^1 dudv T_i^{II}(\omega, v, u) \hat{f}_B \phi_B(\omega) f_{M_1} \phi_{M_1}(v) f_{M_2} \phi_{M_2}(u) \right\}. \quad (1) \end{aligned}$$

The hard-scattering kernel T^I starts from $\mathcal{O}(1)$ and contains all vertex interactions, whereas T^{II} starts from $\mathcal{O}(\alpha_s)$ and comprises hard spectator-interactions. On the basis of the flavour structure of the operators one distinguishes several “topological amplitudes”, which are known completely to next-to-leading order (NLO), i.e. through $\mathcal{O}(\alpha_s)$. The importance of accounting for radiative corrections to the hard-scattering kernels can be clearly seen from the expression for the colour-suppressed tree amplitude, which at NLO reads [1]

$$\alpha_2(\pi\pi) = 0.220 - [0.179 + 0.077 i]_{\text{NLO}} + \left[\frac{r_{\text{sp}}}{0.445} \right] \left\{ [0.114]_{\text{LOsp}} + [0.067]_{\text{tw3}} \right\}. \quad (2)$$

One recognizes the large cancellation between the tree-level and the one-loop vertex correction (denoted by “NLO”), which is due to the fact that the Born term is small because of colour suppression. This suppression is lifted at one-loop due to the appearance of additional colour structures.¹ The last term proportional to r_{sp} is another colour-unsuppressed NLO correction that originates from hard spectator-scattering, which turns

¹This suppression can be lifted only once, and all following terms should be natural in size as expected from a perturbative series. Hence, the size of the one-loop correction does not indicate a breakdown of perturbation theory.

out to be significant as well, and opposite in sign compared to the one-loop vertex correction.

From this discussion it is clear that the colour-suppressed tree amplitude is particularly sensitive to the next-to-next-to-leading order (NNLO), which is one of the reasons for going beyond NLO. This is also motivated by phenomenology since for certain quantities one observes deviations from QCDF predictions with experiment, especially in decay channels which are dominated by α_2 , such as the branching ratio and direct CP asymmetry of $\bar{B} \rightarrow \pi^0 \pi^0$ [5]. It is therefore interesting and desirable to explore whether the NNLO QCDF corrections turn the amplitudes into the right direction to cure discrepancies between theory and experiment. Moreover, since direct CP asymmetries only start from $\mathcal{O}(\alpha_s)$, the $\mathcal{O}(\alpha_s^2)$ terms constitute only the first correction and are therefore needed in order to decrease the scale uncertainty stemming from the leading-order terms.

Part of these $\mathcal{O}(\alpha_s^2)$ contributions is already complete, namely the one-loop hard spectator corrections to T^{II} , for which both the tree [6–8] and penguin [9,10] topologies have been worked out. Later, the imaginary part of the vertex kernel T^I [11,12] was computed. There is clearly a demand for the complete $\mathcal{O}(\alpha_s^2)$ terms since leaving out one of the two terms in the formula (1) in a given order may lead to large unphysical effects, as is evident at NLO from (2). In the present paper we compute the two-loop NNLO corrections to the topological tree amplitudes α_1 and α_2 , including the real and imaginary part, in a fully analytic form. Recently, the so far missing real part also appeared in [13]. What we add, besides confirming a technically highly non-trivial calculation, is an analytic expression for the charm and bottom mass dependence arising from massive quark-loop insertions into the gluon propagator. This should be useful for the NNLO calculation of the remaining penguin amplitudes that we plan to address in a later work [14]. We also discuss the numerical impact of the two-loop correction on $B \rightarrow \pi\pi, \pi\rho, \rho\rho$ branching fractions and branching fraction ratios, updating some results of [5], which are now available with NNLO accuracy. A complementary analysis of these modes at NNLO can be found in [15].

Our article is organized as follows. In Section 2 we introduce the theoretical framework and explain the matching of QCD onto SCET. In Section 3 we describe the techniques applied during the two-loop calculation. In Section 4 we give the master formulas for the hard-scattering kernels, and Section 5 contains the results of their convolution in Gegenbauer moments. The non-leptonic $B \rightarrow \pi\pi, \pi\rho, \rho\rho$ branching fraction and ratio analysis is found in Section 6. We will conclude in Section 7. The lengthy analytic expressions for the unintegrated hard-scattering kernels and a discussion of the two-loop master integrals can be found in two appendices.

2 Theoretical framework, matching QCD to SCET

The starting point of our calculation is the effective weak Hamiltonian where the top quark and the heavy gauge bosons are integrated out [16]. In order to compute the $\mathcal{O}(\alpha_s^2)$ corrections to α_1 and α_2 we need the current-current operators of the Hamilto-

nian. Throughout this paper we work in the Chetyrkin-Misiak-Münz (CMM) operator basis [17] since it allows to consistently use the naive dimensional regularization (NDR) scheme with anticommuting γ_5 . We then have

$$\mathcal{H}_{eff} = \frac{G_F}{\sqrt{2}} V_{ud}^* V_{ub} (C_1 Q_1 + C_2 Q_2) + \text{h.c.}, \quad (3)$$

where

$$\begin{aligned} Q_1 &= \bar{u}\gamma^\mu T^a (1 - \gamma_5) b \bar{d}\gamma_\mu T^a (1 - \gamma_5) u, \\ Q_2 &= \bar{u}\gamma^\mu (1 - \gamma_5) b \bar{d}\gamma_\mu (1 - \gamma_5) u. \end{aligned} \quad (4)$$

Since we will use dimensional regularization the operator basis has to be extended by so-called evanescent operators. They are only non-vanishing for $D \neq 4$ space-time dimensions, and are needed in order to close the operator basis under renormalization. In our case they read

$$\begin{aligned} E_1^{(1)} &= \bar{u}\gamma^\mu \gamma^\nu \gamma^\rho T^a (1 - \gamma_5) b \bar{d}\gamma_\mu \gamma_\nu \gamma_\rho T^a (1 - \gamma_5) u - 16Q_1, \\ E_2^{(1)} &= \bar{u}\gamma^\mu \gamma^\nu \gamma^\rho (1 - \gamma_5) b \bar{d}\gamma_\mu \gamma_\nu \gamma_\rho (1 - \gamma_5) u - 16Q_2, \\ E_1^{(2)} &= \bar{u}\gamma^\mu \gamma^\nu \gamma^\rho \gamma^\sigma \gamma^\lambda T^a (1 - \gamma_5) b \bar{d}\gamma_\mu \gamma_\nu \gamma_\rho \gamma_\sigma \gamma_\lambda T^a (1 - \gamma_5) u - 20E_1^{(1)} - 256Q_1, \\ E_2^{(2)} &= \bar{u}\gamma^\mu \gamma^\nu \gamma^\rho \gamma^\sigma \gamma^\lambda (1 - \gamma_5) b \bar{d}\gamma_\mu \gamma_\nu \gamma_\rho \gamma_\sigma \gamma_\lambda (1 - \gamma_5) u - 20E_2^{(1)} - 256Q_2. \end{aligned} \quad (5)$$

Our computation amounts to performing a matching calculation from QCD onto SCET [18–21], which in the context of spectator scattering has been worked out in [6]. Adopting the notation of that paper for the calculation of the vertex correction means that we determine the matching coefficients of SCET four-quark operators [22]. There are two cases to consider depending on how the quark flavours from the operators (4) flow into the final state. The first possibility is that the d and \bar{u} quarks from the $(\bar{d}u)_{V-A}$ current move in nearly the same direction, and are therefore described by the same type of collinear fields. This gives rise to the colour-allowed topological tree amplitude $\alpha_1(M_1 M_2)$, in which the second meson M_2 carries the flavour quantum numbers of $[\bar{u}d]$. We refer to this as the “right insertion” of the operators (4) [6], and express the matrix elements of Q_i as

$$\langle Q_i \rangle = \sum_a H_{ia} \langle O_a \rangle. \quad (6)$$

The basis of non-local SCET four-quark operators on the right-hand side is given by

$$\begin{aligned} O_1 &= \bar{\chi} \frac{\not{n}_-}{2} (1 - \gamma_5) \chi \bar{\xi} \not{n}_+ (1 - \gamma_5) h_v, \\ O_2 &= \bar{\chi} \frac{\not{n}_-}{2} (1 - \gamma_5) \gamma_\perp^\alpha \gamma_\perp^\beta \chi \bar{\xi} \not{n}_+ (1 - \gamma_5) \gamma_{\perp\beta} \gamma_{\perp\alpha} h_v, \\ O_3 &= \bar{\chi} \frac{\not{n}_-}{2} (1 - \gamma_5) \gamma_\perp^\alpha \gamma_\perp^\beta \gamma_\perp^\gamma \gamma_\perp^\delta \chi \bar{\xi} \not{n}_+ (1 - \gamma_5) \gamma_{\perp\delta} \gamma_{\perp\gamma} \gamma_{\perp\beta} \gamma_{\perp\alpha} h_v. \end{aligned} \quad (7)$$

Our conventions are as follows. Meson M_1 , which picks up the spectator antiquark from the \bar{B} meson, moves into the direction of the light-like vector n_- . The collinear quark field for this direction is ξ , with $\not{n}_-\xi = 0$. The second meson M_2 moves into the opposite light-like direction n_+ . The collinear quark field for this direction is χ , satisfying $\not{n}_+\chi = 0$. The effective heavy-quark field is labelled by the time-like vector $v = (n_+ + n_-)/2$ with $v^2 = 1$ as usual, and satisfies $\not{v}h_v = h_v$. The perpendicular component of any four-vector, including Dirac matrices, is defined by

$$p^\mu = n_+ \cdot p \frac{n_-^\mu}{2} + n_- \cdot p \frac{n_+^\mu}{2} + p_\perp^\mu. \quad (8)$$

The SCET operators O_i are actually non-local on the light-cone, the n_+ -collinear part being of the form $\bar{\chi}(tn_-)[\dots]\chi(0)$. The matching coefficients H_{ia} in (6) are therefore functions of a single variable, usually chosen to be the Fourier conjugate of t , and the product $H_{ia} \langle O_a \rangle$ must be interpreted as a convolution product. The non-locality, as well as the collinear Wilson lines that render the non-local product $\bar{\chi}(tn_-)[\dots]\chi(0)$ gauge-invariant, and also the quark flavour, are not indicated explicitly in (7). We refer to [6] for further technical details concerning these issues.

The second possibility, called “wrong insertion”, arises when the u quark from the $(\bar{u}b)_{V-A}$ current and \bar{u} quark from the $(\bar{d}u)_{V-A}$ current move in nearly the same direction. The corresponding amplitude is the colour-suppressed tree amplitude $\alpha_2(M_1M_2)$ and meson M_2 is now made up of $[\bar{u}u]$. To obtain this amplitude, the QCD operators are matched to SCET via

$$\langle Q_i \rangle = \sum_a \tilde{H}_{ia} \langle \tilde{O}_a \rangle, \quad (9)$$

where now the basis consists of

$$\begin{aligned} \tilde{O}_1 &= \bar{\xi} \gamma_\perp^\alpha (1 - \gamma_5) \chi \bar{\chi} (1 + \gamma_5) \gamma_{\perp\alpha} h_v, \\ \tilde{O}_2 &= \bar{\xi} \gamma_\perp^\alpha \gamma_\perp^\beta \gamma_\perp^\gamma (1 - \gamma_5) \chi \bar{\chi} (1 + \gamma_5) \gamma_{\perp\alpha} \gamma_{\perp\gamma} \gamma_{\perp\beta} h_v, \\ \tilde{O}_3 &= \bar{\xi} \gamma_\perp^\alpha \gamma_\perp^\beta \gamma_\perp^\gamma \gamma_\perp^\delta \gamma_\perp^\epsilon (1 - \gamma_5) \chi \bar{\chi} (1 + \gamma_5) \gamma_{\perp\alpha} \gamma_{\perp\epsilon} \gamma_{\perp\delta} \gamma_{\perp\gamma} \gamma_{\perp\beta} h_v. \end{aligned} \quad (10)$$

Note that the χ fields, which carry the flavour of M_2 , now stand in two different fermion bilinears, hence the name “wrong insertion”. The remarks above on non-locality apply to these operators as well.

The SCET operators in (7) and (10) are constructed such that all operators with indices 2 and 3 are evanescent, i.e. they vanish in $D = 4$ dimensions. Moreover, \tilde{O}_1 is Fierz equivalent to O_1 in $D = 4$ dimensions. Hence, we treat the difference $\tilde{O}_1 - O_1$ as another evanescent operator, and regard O_1 as the only physical SCET operator. Due to the absence of soft-gluon interactions between collinear fields in different directions in the leading-power SCET Lagrangian after a field redefinition [19], O_1 factorizes into a $(\bar{\chi}\chi)$ part, whose SCET matrix element is a light-cone distribution amplitude, and a $(\bar{\xi}h_v)$ part, which defines the soft part of a heavy-to-light form factor [23, 24].

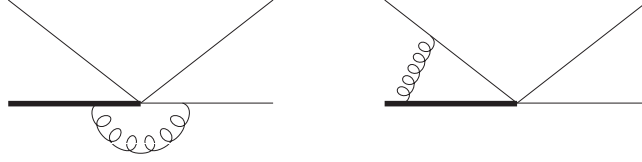


Figure 1: Examples of factorizable (left) and non-factorizable (right) diagrams. By definition, in the former gluon lines do not connect the horizontal with the sloped lines (quarks that go into M_2), in the latter they do connect them. The bold line denotes the bottom quark.

On the QCD side of the matching relations (6), (9) we can write the perturbative expansion of the renormalized matrix elements as

$$\begin{aligned}
\langle Q_i \rangle = & \left\{ A_{ia}^{(0)} + \frac{\alpha_s}{4\pi} \left[A_{ia}^{(1)} + Z_{ext}^{(1)} A_{ia}^{(0)} + Z_{ij}^{(1)} A_{ja}^{(0)} \right] \right. \\
& + \left(\frac{\alpha_s}{4\pi} \right)^2 \left[A_{ia}^{(2)} + Z_{ij}^{(1)} A_{ja}^{(1)} + Z_{ij}^{(2)} A_{ja}^{(0)} + Z_{ext}^{(1)} A_{ia}^{(1)} + Z_{ext}^{(2)} A_{ia}^{(0)} \right. \\
& \left. \left. + Z_{ext}^{(1)} Z_{ij}^{(1)} A_{ja}^{(0)} + Z_{\alpha}^{(1)} A_{ia}^{(1)} + (-i) \delta m^{(1)} A_{ia}^{\prime(1)} \right] + \mathcal{O}(\alpha_s^3) \right\} \langle O_a \rangle^{(0)} \quad (11)
\end{aligned}$$

for the right insertion, and for the wrong insertion we simply replace $A \rightarrow \tilde{A}$ and $O \rightarrow \tilde{O}$. In (11), and throughout the paper, α_s denotes the strong coupling in the $\overline{\text{MS}}$ scheme with five active quark flavours at the scale μ , and a superscript on any quantity S will label the order in α_s according to

$$S = S^{(0)} + \frac{\alpha_s}{4\pi} S^{(1)} + \left(\frac{\alpha_s}{4\pi} \right)^2 S^{(2)} + \mathcal{O}(\alpha_s^3). \quad (12)$$

The renormalization factors Z_{ij} , Z_{α} , δm , and Z_{ext} account for operator, coupling, mass, and wave-function renormalization, respectively. We will give more details on them in Section 4. The $A_{ia}^{(\ell)}$ in (11) denote bare ℓ -loop on-shell matrix elements of the operators Q_i in the effective weak Hamiltonian. For $\ell = 2$ we only need $i = 1, 2$, but for $\ell < 2$ we need in addition the tree-level and one-loop matrix elements of the evanescent operators due to terms such as $Z_{ij}^{(1)} A_{ja}^{(1)}$ in (11). The amplitudes $A_{ia}^{(\ell)}$ can be further split up into factorizable and non-factorizable diagrams, see Figure 1, according to

$$A_{ia}^{(\ell)} = A_{ia}^{(\ell)f} + A_{ia}^{(\ell)nf}, \quad (13)$$

which turns out to be convenient since in the matching procedure the factorizable diagrams will cancel to a large extent.

On the SCET side of the matching relation the matrix elements of O_a assume a similar form to (11), but there is no mass counterterm for a HQET quark, and the

coupling is renormalized in the four-flavour theory (denoted by a hat on the coupling and renormalization constant),

$$\begin{aligned} \langle O_a \rangle = & \left\{ \delta_{ab} + \frac{\hat{\alpha}_s}{4\pi} \left[M_{ab}^{(1)} + Y_{ext}^{(1)} \delta_{ab} + Y_{ab}^{(1)} \right] + \left(\frac{\hat{\alpha}_s}{4\pi} \right)^2 \left[M_{ab}^{(2)} + Y_{ac}^{(1)} M_{cb}^{(1)} + Y_{ab}^{(2)} \right. \right. \\ & \left. \left. + Y_{ext}^{(1)} M_{ab}^{(1)} + Y_{ext}^{(2)} \delta_{ab} + Y_{ext}^{(1)} Y_{ab}^{(1)} + \hat{Z}_\alpha^{(1)} M_{ab}^{(1)} \right] + \mathcal{O}(\alpha_s^3) \right\} \langle O_b \rangle^{(0)}. \end{aligned} \quad (14)$$

The amplitudes are now labelled $M_{ab}^{(\ell)}$, and Y are the SCET renormalization constants. Again, the corresponding formula for the wrong insertion is obtained by obvious replacements. When dimensional regularization is used as IR regulator the on-shell renormalization constants are equal to unity and the bare matrix elements are zero except for the two-loop diagrams with a massive charm quark-loop insertion,

$$\langle O_a \rangle = \left\{ \delta_{ab} + \frac{\hat{\alpha}_s}{4\pi} Y_{ab}^{(1)} + \left(\frac{\hat{\alpha}_s}{4\pi} \right)^2 \left[M_{ab}^{(2)} + Y_{ab}^{(2)} \right] + \mathcal{O}(\alpha_s^3) \right\} \langle O_b \rangle^{(0)}. \quad (15)$$

This expression assumes that we determined the operator ultraviolet renormalization factors Y_{ab} from the general expression (14), using another regulator than dimensional for the infrared divergences, but then use (15) in the matching relation since the QCD side (11) is calculated with dimensional regularization as infrared regulator. In this relation we eliminate the four-flavour coupling by the D -dimensional relation $\hat{\alpha}_s = \xi_{45}^{-1} \alpha_s$, where $\xi_{45} = 1 + \mathcal{O}(\alpha_s)$ is expanded as in (12). Since the SCET operators depend on a variable, the renormalization factors $Y_{ab} = Y_{ab}(u, u')$ are functions of two variables and the product in (15) is a convolution.

Just as for four-quark operators, we can write down a matching equation for QCD *currents* to SCET *currents*. This is convenient since in this way we can organize the calculation such that the factorizable diagrams are cancelled, at least for the right insertion. We consider the relations²

$$\begin{aligned} \bar{q} \frac{\not{h}_-}{2} (1 - \gamma_5) q &= C_{\bar{q}q} \bar{\chi} \frac{\not{h}_-}{2} (1 - \gamma_5) \chi, \\ \bar{q} \not{h}_+ (1 - \gamma_5) b &= C_{FF} \bar{\xi} \not{h}_+ (1 - \gamma_5) h_v. \end{aligned} \quad (16)$$

Since a single collinear sector in SCET is equivalent to full QCD [20] we have $C_{\bar{q}q} = 1 + \mathcal{O}(\alpha_s^2)$ because diagrams with massive bottom quark loops (not contained in SCET) arise only at two loops and beyond. The matching coefficient C_{FF} can be determined from matching calculations for the $b \rightarrow u$ transition [18, 25–29]. In the notation of [28] we have

$$C_{FF} = C_1 + \frac{u}{2} C_2 + C_3 \Big|_{u=1} = 1 - \frac{\alpha_s}{4\pi} \frac{C_F}{12} (6L^2 + 30L + \pi^2 + 72) + \mathcal{O}(\alpha_s^2), \quad (17)$$

²The first relation is somewhat schematic, since we suppressed the non-locality of the operator and the Wilson line connecting the quark fields on both sides of the equation.

with

$$L \equiv \ln \left(\frac{\mu^2}{m_b^2} \right). \quad (18)$$

From (16) one can construct the following factorized QCD operator

$$O_{\text{QCD}} \equiv \left[\bar{q} \frac{\not{\eta}_-}{2} (1 - \gamma_5) q \right] \left[\bar{q} \not{\eta}_+ (1 - \gamma_5) b \right] = C_{FF} C_{\bar{q}q} O_1, \quad (19)$$

which is *defined* by the product of the two currents given above. By construction the matrix element of the factorized QCD operator is the product of a light-cone distribution amplitude and the *full QCD* form factor. In terms of this operator the matrix elements of Q_i read for the right and wrong insertion, respectively,

$$\langle Q_i \rangle = T_i \langle O_{\text{QCD}} \rangle + \sum_{a>1} H_{ia} \langle O_a \rangle, \quad (20)$$

$$\langle Q_i \rangle = \tilde{T}_i \langle O_{\text{QCD}} \rangle + \tilde{H}_{i1} \langle \tilde{O}_1 - O_1 \rangle + \sum_{a>1} \tilde{H}_{ia} \langle \tilde{O}_a \rangle. \quad (21)$$

Comparing (20) and (21) with (6) and (9) one finally obtains for the hard-scattering kernels

$$T_i = \frac{H_{i1}}{C_{FF} C_{\bar{q}q}}, \quad \tilde{T}_i = \frac{\tilde{H}_{i1}}{C_{FF} C_{\bar{q}q}}. \quad (22)$$

3 Computational methods

The calculation of the two-loop QCD amplitude involves the evaluation of the 62 non-factorizable diagrams shown in Figures 15 and 16 of [2]. In addition, there are four diagrams which involve a gluon self-energy, and in each of these the self-energy loop comprises massless quarks, gluons, ghosts, and the massive charm and bottom quarks.

We work in dimensional regularization with $D = 4 - 2\epsilon$, where UV and IR (soft and collinear) divergences appear as poles of up to the fourth order in ϵ . Since we work in the CMM basis we can adopt for γ_5 consistently the NDR scheme with fully anticommuting γ_5 .

The amplitude of the diagrams is reduced by techniques that have become standard in multi-loop calculations. We apply a Passarino – Veltman [30] reduction to the vector and tensor integrals. The Dirac and color algebra is then performed by means of an in-house Mathematica routine. The dimensionally regularized scalar integrals are further reduced to a small set of master integrals using the Laporta algorithm [31, 32] based on integration-by-parts (IBP) identities [33, 34]. To this end we use the package AIR [35].

The techniques we apply during the evaluation of the master integrals are manifold. The easier integrals can be written in closed form in terms of Γ -functions and hypergeometric functions and can subsequently be expanded in ϵ with the package HypExp [36, 37]. In more complicated cases we derive Mellin-Barnes representations by means of the

package AMBRE [38]. We perform the analytic continuation to $\epsilon = 0$ with the package MB [39], which is also used for numerical cross-checks. We then apply Barnes' lemmas and the theorem of residues to the multiple Mellin-Barnes integrals, and insert integral representations of hypergeometric functions as well as ψ -functions and Euler's B -function where appropriate. As a third technique we apply the method of differential equations [40–42] and evaluate the boundary condition with the Mellin-Barnes technique. Eventually, the master integrals are evaluated as Laurent series in ϵ .

The master integrals of all diagrams except the ones in which the gluon self-energy contains a charm-quark loop are obtained in a fully analytic form. The coefficient functions of the Laurent series in ϵ are logarithms, polylogarithms and harmonic polylogarithms [43] of maximum weight four. Two master integrals of the diagrams with a charm loop in the gluon self-energy cannot be displayed in a purely analytic form, see (76) and (78). Hence the charm-dependent part of the hard-scattering kernels still contains two-fold auxiliary integrals, see (93), (77), and (79). However, after convolution of the hard-scattering functions with the Gegenbauer expansion of the light-cone distribution amplitudes, we obtain fully analytic results, including the charm-mass dependence, for the topological tree amplitudes α_1 and α_2 .

The master integrals have been calculated already in [11] and they have been used in [12]. We find perfect agreement on the expressions given in [11]. Nevertheless, we give in Appendix A explicitly the results of a selected subset of master integrals. The reason for this is that we found closed forms valid to all orders in ϵ , or that we need the structure of the result for the hard-scattering kernels and the topological tree amplitudes derived in the subsequent sections.

4 Master formulas

From the equations given in Section 2 we can deduce the master formulas for the hard-scattering kernels. Expanding them according to

$$T_i = T_i^{(0)} + \frac{\alpha_s}{4\pi} T_i^{(1)} + \left(\frac{\alpha_s}{4\pi}\right)^2 T_i^{(2)} + \mathcal{O}(\alpha_s^3), \quad (23)$$

where α_s denotes the five-flavour coupling in the $\overline{\text{MS}}$ scheme, the master formula for the hard-scattering kernels for the right insertion reads

$$\begin{aligned} T_i^{(0)} &= A_{i1}^{(0)}, \\ T_i^{(1)} &= A_{i1}^{(1)\text{nf}} + Z_{ij}^{(1)} A_{j1}^{(0)}, \\ T_i^{(2)} &= A_{i1}^{(2)\text{nf}} + Z_{ij}^{(1)} A_{j1}^{(1)} + Z_{ij}^{(2)} A_{j1}^{(0)} + Z_\alpha^{(1)} A_{i1}^{(1)\text{nf}} + (-i) \delta m^{(1)} A_{i1}'^{(1)\text{nf}} \\ &\quad - T_i^{(1)} [C_{FF}^{(1)} + Y_{11}^{(1)} - Z_{ext}^{(1)}] - \sum_{b>1} H_{ib}^{(1)} Y_{b1}^{(1)}. \end{aligned} \quad (24)$$

The actual calculation amounts to evaluating the two-loop on-shell matrix element of the transition $b(p) \rightarrow q_1(p')q_2(uq)\bar{q}_3(\bar{u}q)$ with kinematics $p = p' + q$, $p^2 = m_b^2$, $p'^2 = q^2 = 0$,

and u ($\bar{u} = 1 - u$) the momentum fraction of the quark (antiquark) in M_2 . Thus, $T_i^{(\ell)}$, $A_{k1}^{(\ell)}$ and $H_{ib}^{(\ell)}$ depend on u , and a term involving $Y_{ab}^{(\ell)}$ such as $H_{ib}^{(1)} Y_{b1}^{(1)}$ must be interpreted as the convolution product $\int_0^1 du' H_{ib}^{(1)}(u') Y_{b1}^{(1)}(u', u)$.

While the individual terms on the right-hand side of (24) may be divergent, the hard-scattering kernels are free of poles in ϵ . In general, we need tree-level and one-loop quantities such as $A_{j1}^{(0)}$, $T_i^{(1)}$, $A_{j1}^{(1)}$ etc. to order $\mathcal{O}(\epsilon)$ (and even $\mathcal{O}(\epsilon^2)$ for $A_{j1}^{(0)}$ and $T_i^{(1)}$), since they multiply divergent renormalization constants in the expression for the two-loop hard-scattering function $T_i^{(2)}$. The Z_{ij} are the operator renormalization constants from the effective weak Hamiltonian. Their matrix expressions read [44, 45]

$$\begin{aligned}
Z^{(1)} &= \frac{1}{\epsilon} \begin{pmatrix} -2 & \frac{4}{3} & \frac{5}{12} & \frac{2}{9} & 0 & 0 \\ 6 & 0 & 1 & 0 & 0 & 0 \end{pmatrix}, \\
Z^{(2)} &= \frac{1}{\epsilon^2} \begin{pmatrix} -\frac{4T_f n_f}{3} + 17 & \frac{8T_f n_f}{9} - \frac{26}{3} & \frac{5T_f n_f}{18} - \frac{25}{6} & \frac{4T_f n_f}{27} - \frac{31}{18} & \frac{19}{96} & \frac{5}{108} \\ 4T_f n_f - 39 & 4 & \frac{2T_f n_f}{3} - \frac{31}{4} & 0 & \frac{5}{24} & \frac{1}{9} \end{pmatrix} \\
&\quad + \frac{1}{\epsilon} \begin{pmatrix} \frac{8T_f n_f}{9} + \frac{79}{12} & \frac{20T_f n_f}{27} - \frac{205}{18} & -\frac{5T_f n_f}{108} + \frac{1531}{288} & -\frac{2T_f n_f}{81} - \frac{1}{72} & \frac{1}{384} & -\frac{35}{864} \\ \frac{10T_f n_f}{3} + \frac{83}{4} & 3 & -\frac{T_f n_f}{9} + \frac{119}{16} & \frac{8}{9} & -\frac{35}{192} & -\frac{7}{72} \end{pmatrix}, \tag{25}
\end{aligned}$$

where $n_f = n_l + 1 = 5$ is the total number of quark flavours, and $T_f = 1/2$. The row index of the matrices $Z^{(1)}$ and $Z^{(2)}$ labels $(Q_1, Q_2, E_1^{(1)}, E_2^{(1)}, E_1^{(2)}, E_2^{(2)})$, whereas the column index stands for (Q_1, Q_2) . Hence in all terms of the form $Z_{ij} A_{j1}$ we also have to consider the matrix elements of the evanescent operators, including the factorizable diagrams. The terms proportional to $Z_\alpha^{(1)}$, $\delta m^{(1)}$, and $Z_{ext}^{(1)}$ account for coupling, mass, and wave function renormalization, respectively. The coupling is renormalized in the $\overline{\text{MS}}$ scheme with five active quark flavours, whereas the mass and the wave-functions are renormalized in the on-shell scheme. The term C_{FF} was already discussed in the previous section. The SCET renormalization kernel $Y_{11}^{(1)}$ factorizes according to

$$Y_{11}^{(1)}(u, u') = Z_J^{(1)} \delta(u - u') + Z_{BL}^{(1)}(u, u') \tag{26}$$

into the universal renormalization factor for SCET currents,

$$Z_J^{(1)} = C_F \left\{ -\frac{1}{\epsilon^2} + \frac{1}{\epsilon} \left[-L - \frac{5}{2} \right] \right\}, \tag{27}$$

and the contribution from the ERBL [46, 47] kernel, for which we use the convention of Eq. (51) in [48]. The last term in (24) emerges from the fact that the SCET evanescent operators $O_{2,3}$ mix into O_1 . Renormalizing the evanescent operator matrix elements to zero introduces the finite off-diagonal renormalization constants $Y_{b1}^{(1)}$. As a consequence, we also have to calculate the one-loop hard-scattering kernels of the evanescent operators, $H_{ib}^{(1)}$, $b > 1$, for which only $b = 2$ arises at this order. We find that only the diagram with gluon exchange between the n_+ -collinear quark and antiquark lines contributes to

the off-diagonal renormalization constant $Y_{21}^{(1)}$, as was the case in a related calculation performed for the spectator-scattering kernels in [6]. The required convolution results in

$$\begin{aligned}
-\sum_{b=2,3} H_{1b}^{(1)} Y_{b1}^{(1)} &= -\frac{64L}{9} - \frac{800}{27} + \frac{16\pi^2}{27(1-u)} + \frac{16\pi^2}{27u} + \frac{32\ln(1-u)}{9} + \frac{32\ln(u)}{9} \\
&\quad - \frac{32\text{Li}_2(1-u)}{9u} - \frac{32\text{Li}_2(u)}{9(1-u)} - \frac{32i\pi}{9}
\end{aligned} \tag{28}$$

for $i = 1$; it vanishes for $i = 2$.

The master formula for the expansion of the wrong insertion hard-scattering kernels reads

$$\begin{aligned}
\tilde{T}_i^{(0)} &= \tilde{A}_{i1}^{(0)}, \\
\tilde{T}_i^{(1)} &= \tilde{A}_{i1}^{(1)\text{nf}} + Z_{ij}^{(1)} \tilde{A}_{j1}^{(0)} + \underbrace{\tilde{A}_{i1}^{(1)\text{f}} - A_{21}^{(1)\text{f}} \tilde{A}_{i1}^{(0)}}_{\mathcal{O}(\epsilon)} - \underbrace{[\tilde{Y}_{11}^{(1)} - Y_{11}^{(1)}] \tilde{A}_{i1}^{(0)}}_{\mathcal{O}(\epsilon)}, \\
\tilde{T}_i^{(2)} &= \tilde{A}_{i1}^{(2)\text{nf}} + Z_{ij}^{(1)} \tilde{A}_{j1}^{(1)} + Z_{ij}^{(2)} \tilde{A}_{j1}^{(0)} + Z_\alpha^{(1)} \tilde{A}_{i1}^{(1)\text{nf}} \\
&\quad + (-i) \delta m^{(1)} \tilde{A}_{i1}^{(1)\text{nf}} + Z_{ext}^{(1)} [\tilde{A}_{i1}^{(1)\text{nf}} + Z_{ij}^{(1)} \tilde{A}_{j1}^{(0)}] \\
&\quad - \tilde{T}_i^{(1)} [C_{FF}^{(1)} + \tilde{Y}_{11}^{(1)}] - \sum_{b>1} \tilde{H}_{ib}^{(1)} \tilde{Y}_{b1}^{(1)} \\
&\quad + [\tilde{A}_{i1}^{(2)\text{f}} - A_{21}^{(2)\text{f}} \tilde{A}_{i1}^{(0)}] + (-i) \delta m^{(1)} [\tilde{A}_{i1}^{(1)\text{f}} - A_{21}^{(1)\text{f}} \tilde{A}_{i1}^{(0)}] \\
&\quad + (Z_\alpha^{(1)} + Z_{ext}^{(1)}) [\tilde{A}_{i1}^{(1)\text{f}} - A_{21}^{(1)\text{f}} \tilde{A}_{i1}^{(0)}] \\
&\quad - [\tilde{M}_{11}^{(2)} - M_{11}^{(2)}] \tilde{A}_{i1}^{(0)} \\
&\quad - (C_{FF}^{(1)} - \xi_{45}^{(1)}) [\tilde{Y}_{11}^{(1)} - Y_{11}^{(1)}] \tilde{A}_{i1}^{(0)} - [\tilde{Y}_{11}^{(2)} - Y_{11}^{(2)}] \tilde{A}_{i1}^{(0)}.
\end{aligned} \tag{29}$$

All terms in the first three lines of $\tilde{T}_i^{(2)}$ have a corresponding term in the master formula (24) for the right insertion. The fourth and fifth lines describe Fierz differences of factorizable QCD diagrams not contained in the QCD form factor or LCDA. The sixth line stems from two-loop SCET matrix elements with a massive charm-loop insertion. The terms in the last line of (29) emerge from the fact that the difference $\tilde{O}_1 - O_1$ is evanescent and hence we must renormalize its matrix element to zero. Similar terms already appear in the one-loop expression $\tilde{T}_i^{(1)}$, in which case, however, they are $\mathcal{O}(\epsilon)$, as indicated, and can be dropped.

In the two-loop expression, we here find $-\sum_{b>1} \tilde{H}_{ib}^{(1)} \tilde{Y}_{b1}^{(1)} = 0$, since the mixing of \tilde{O}_2 into \tilde{O}_1 at one-loop is of higher order in ϵ . The terms in the fourth to the last line of the expression for $\tilde{T}_i^{(2)}$ in (29), which appear only for the wrong insertion, are given

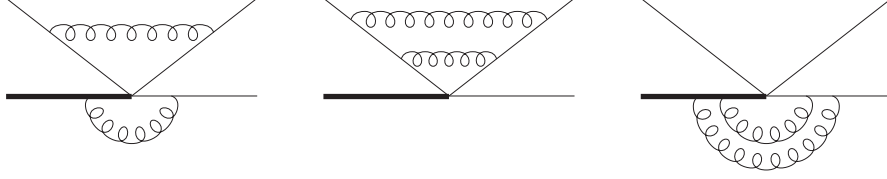


Figure 2: Examples of factorizable diagrams of class A (left), B (center), and C (right).

explicitly for $i = 1^3$ as follows:

$$\tilde{A}_{11}^{(2)f} - A_{21}^{(2)f} \tilde{A}_{11}^{(0)} = \frac{64}{81\epsilon} + \frac{128L}{81} + \frac{32}{81} n_l T_f - \frac{32}{81} T_f + \frac{56}{81}, \quad (30)$$

$$(Z_\alpha^{(1)} + Z_{ext}^{(1)})[\tilde{A}_{11}^{(1)f} - A_{21}^{(1)f} \tilde{A}_{11}^{(0)}] = -\frac{64}{81} n_l T_f - \frac{64}{81} T_f + \frac{208}{27}, \quad (31)$$

$$(-i) \delta m^{(1)} [\tilde{A}'_{11}{}^{(1)f} - A'_{21}{}^{(1)f} \tilde{A}_{11}^{(0)}] = \mathcal{O}(\epsilon), \quad (32)$$

$$-[\tilde{M}_{11}^{(2)} - M_{11}^{(2)}] \tilde{A}_{11}^{(0)} = \frac{32}{81} T_f, \quad (33)$$

$$-(C_{FF}^{(1)} - \xi_{45}^{(1)})[\tilde{Y}_{11}^{(1)} - Y_{11}^{(1)}] \tilde{A}_{11}^{(0)} = \mathcal{O}(\epsilon), \quad (34)$$

$$[(\tilde{Y}_{11}^{(1)} - Y_{11}^{(1)}) \tilde{Y}_{11}^{(1)} - (\tilde{Y}_{11}^{(2)} - Y_{11}^{(2)})] \tilde{A}_{11}^{(0)} = -\frac{32}{81} n_l T_f + \frac{136}{81}. \quad (35)$$

Let us elaborate more on (30) – (35). In (30) we have to calculate the factorizable two-loop diagrams both, for the right and the wrong insertion. Since the two are related by a Fierz transformation, many terms drop out, resulting in the simple expression (30). There are three classes of two-loop diagrams that contribute to (30). They are labelled class A, B, and C, respectively, and examples are shown in Figure 2. Diagrams of class A do not contribute to the on-shell matrix elements since scaleless integrals vanish in dimensional regularization. For the same reason, only those diagrams of class B contribute that contain a massive quark loop insertion in the gluon propagator. Diagrams of class C have to be evaluated explicitly, and their right-insertion result can be checked against the two-loop heavy-to-light current matching calculation at the kinematic endpoint [26–29]. In (31) the renormalization constants multiply the Fierz difference of the one-loop factorizable diagram, and in (32) we evaluate the Fierz difference of the one-loop factorizable diagram with a mass counterterm insertion on the heavy line; the latter turns out to be of $\mathcal{O}(\epsilon)$. Eq. (33) comprises the Fierz difference of two-loop on-shell SCET diagrams with a charm-loop insertion into a gluon propagator. In order to determine the SCET renormalization constants $Y_{11}^{(\ell)}$ and $\tilde{Y}_{11}^{(\ell)}$ in (34) and (35), we must use an IR regulator different from the dimensional one. The difference $\tilde{Y}_{11}^{(1)} - Y_{11}^{(1)}$ must then be a finite, regulator-independent constant. However, it turns out that this difference is $\mathcal{O}(\epsilon)$, hence there is no contribution to $\tilde{T}_i^{(2)}$ from (34).

³The corresponding terms for $i = 2$ are in these cases obtained by removing a factor of $C_F = 4/3$.

The last term (35), which does not appear in this form in (29), requires further explanation. While $Y_{11}^{(\ell)}$ is a $\overline{\text{MS}}$ renormalization constant for the physical SCET operator O_1 , $\tilde{Y}_{11}^{(\ell)}$ is a non-minimal renormalization factor determined by the requirement that the matrix element of the evanescent operator $\tilde{O}_1 - O_1$ vanishes. As a consequence, $\tilde{Y}_{11}^{(1)} - Y_{11}^{(1)}$ depends on the (non-dimensional) infrared regulator at $\mathcal{O}(\epsilon^2)$, and so does the finite term of the two-loop renormalization factor $\tilde{Y}_{11}^{(2)} - Y_{11}^{(2)}$, for example from a diagram such as the first one in Figure 2. The infrared regulator dependence of $\tilde{Y}_{11}^{(1)} - Y_{11}^{(1)}$ enters the $\mathcal{O}(\epsilon^2)$ terms of $\tilde{T}_i^{(1)}$ as can be seen from (29), and subsequently the finite term of $\tilde{T}_i^{(2)}$ through $\tilde{T}_i^{(1)}\tilde{Y}_{11}^{(1)}$. Of course, the final result for $\tilde{T}_i^{(2)}$ must be independent of this regulator. To see this we extract the infrared-sensitive $\mathcal{O}(\epsilon^2)$ term from $\tilde{T}_i^{(1)}$ by decomposing it in the form $\tilde{T}_i^{(1)} = \tilde{T}_i^{(1)F} - [\tilde{Y}_{11}^{(1)} - Y_{11}^{(1)}]\tilde{T}_i^{(0)}$ and combine the subtracted term with $-[\tilde{Y}_{11}^{(2)} - Y_{11}^{(2)}]\tilde{A}_{i1}^{(0)}$ from (29). This results in the left-hand side of (35). We then calculate the combination of renormalization factors that appears in this equation and obtain the infrared-finite result given above. For this calculation we used two different methods. One applies the method of IR-rearrangement similar to [49, 50]. The other combines terms algebraically such that no infrared regulator has to be introduced to calculate (35). In this way we also verify that the finite term is regulator independent. Summing all terms we find that $\tilde{T}_i^{(2)}$ is infrared and ultraviolet finite as required by the factorization theorem.

The final result for the hard-scattering kernels is lengthy and complicated. We therefore relegate the explicit expressions for the right-insertion kernels $T_i^{(1)}$ and $T_i^{(2)}$ ($i = 1, 2$) to Appendix B.1.⁴ It turns out that the result of the calculation of the wrong-insertion kernels can be written as linear combination of the right-insertion ones and a residual constant as follows:

$$\begin{aligned}
\tilde{T}_1^{(1)} &= -\frac{1}{3}T_1^{(1)} - \frac{4}{3}, \\
\tilde{T}_2^{(1)} &= 2T_1^{(1)}, \\
\tilde{T}_1^{(2)} &= -\frac{1}{3}T_1^{(2)} + \frac{4}{9}T_2^{(2)} - \frac{20}{27}n_l T_f - \frac{20}{27}T_f - \frac{49}{9}, \\
\tilde{T}_2^{(2)} &= 2T_1^{(2)} + \frac{1}{3}T_2^{(2)} + 6T_1^{(1)}.
\end{aligned} \tag{36}$$

5 Convolution in Gegenbauer moments

For the topological tree amplitudes to NNLO we adopt the following notation

$$\alpha_i(M_1 M_2) = \sum_j C_j V_{ij}^{(0)} + \sum_{l \geq 1} \left(\frac{\alpha_s}{4\pi}\right)^l \left[\frac{C_F}{2N_c} \sum_j C_j V_{ij}^{(l)} + P_i^{(l)} \right] + \dots, \tag{37}$$

⁴Note that the appendix contains the one-loop kernels explicitly only through order $\mathcal{O}(\epsilon^0)$, although their higher order terms enter the two-loop master formulas.

where the ellipsis stands for contributions from hard spectator-scattering which are not subject of the present paper. As before α_s denotes the five-flavour coupling in the $\overline{\text{MS}}$ scheme. The quantities V_{ij} are convolutions of the hard-scattering kernels with the light-cone distribution amplitude of a light meson,

$$\begin{aligned}
V_{1j}^{(0)} &= \int_0^1 du T_j^{(0)} \phi_M(u), \\
V_{2j}^{(0)} &= \int_0^1 du \tilde{T}_j^{(0)} \phi_M(u), \\
\frac{C_F}{2N_c} V_{1j}^{(l)} &= \int_0^1 du T_j^{(l)}(u) \phi_M(u), \\
\frac{C_F}{2N_c} V_{2j}^{(l)} &= \int_0^1 du \tilde{T}_j^{(l)}(u) \phi_M(u).
\end{aligned} \tag{38}$$

The light-cone distribution amplitude of a light meson, ϕ_M , is expanded into the eigenfunctions of the one-loop renormalization kernel,

$$\phi_M(u) = 6u(1-u) \left[1 + \sum_{n=1}^{\infty} a_n^M C_n^{(3/2)}(2u-1) \right], \tag{39}$$

where a_n^M and $C_n^{(3/2)}(x)$ are the Gegenbauer moments and polynomials, respectively, and the integrals (38) are then performed term by term. Below we provide integrated results truncating the Gegenbauer expansion (39) at $n = 2$, which is sufficient in practice. The light-cone distribution amplitude and Gegenbauer moments are scale-dependent, and our notation is such that a_n^M refers to the scale μ that is also the scale of α_s . Since $\phi_M(u)$ is normalized to unity and the tree-level scattering kernels are constant, we simply have

$$\begin{aligned}
V_{11}^{(0)} &= 0, & V_{21}^{(0)} &= \frac{4}{9}, \\
V_{12}^{(0)} &= 1, & V_{22}^{(0)} &= \frac{1}{3}.
\end{aligned} \tag{40}$$

At the one-loop level, one obtains

$$\begin{aligned}
V_{11}^{(1)} &= -\frac{45}{2} - 6L - 3i\pi + \left(\frac{11}{2} - 3i\pi \right) a_1^M - \frac{21}{20} a_2^M, \\
V_{12}^{(1)} &= 0, \\
V_{21}^{(1)} &= -\frac{1}{3} V_{11}^{(1)} - 6, \\
V_{22}^{(1)} &= 2 V_{11}^{(1)}.
\end{aligned} \tag{41}$$

Note that from one-loop onwards, the constants in the V_{ij} are scheme dependent and hence look different in the CMM basis compared to those in the traditional basis [16] employed in the earlier QCD factorization calculations. This explains the different constant in $V_{11}^{(1)}$ compared to the corresponding expression V_M in [3].

At two loops the expressions get more complicated. In order not to spoil the simple structure of the result we split the $V_{ij}^{(2)}$ according to

$$V_{ij}^{(2)} \equiv V_{ij}^{(2)} \Big|_{m_c=0} + T_f \Delta V_{ij}^{(2)} \Big|_{m_c}. \quad (42)$$

The first term on the right-hand side describes the result for a massless charm quark. The second term is the difference between the contribution of a quark of mass m_c and a massless quark, see also (84). This construction ensures that we set $n_l = 4$ irrespective of whether we treat the charm quark as massive or massless. Explicitly, we have

$$\begin{aligned} V_{11}^{(2)} \Big|_{m_c=0} = & \left\{ -39L^2 - 234L + 8194\zeta(5) - 2028\pi^2\zeta(3) - \frac{100862\zeta(3)}{15} + 44\pi^2 \ln(2) \right. \\ & - \frac{55\pi^4}{216} + \frac{43909\pi^2}{18} - \frac{172597}{180} + n_l T_f \left(4L^2 + \frac{70L}{3} - \frac{4\pi^2}{3} + \frac{493}{9} \right) \\ & + T_f \left(4L^2 + \frac{70L}{3} + \frac{56\pi^4}{75} - \frac{164\pi^2}{3} + \frac{1321}{9} + \frac{4128}{5}\zeta(3) \right. \\ & \left. \left. - \frac{92}{5}\pi^2\sqrt{5} - \frac{288}{5}\pi^2 \ln\left(\frac{1}{2} + \frac{\sqrt{5}}{2}\right) \right) \right. \\ & + i\pi \left[-39L - \frac{20\zeta(3)}{3} + \frac{1301\pi^2}{270} - \frac{1591}{9} + n_l T_f \left(4L + \frac{44}{3} \right) \right. \\ & \left. \left. + T_f \left(4L + \frac{932}{3} - 184\sqrt{5} \ln\left(\frac{1}{2} + \frac{\sqrt{5}}{2}\right) - 288 \ln^2\left(\frac{1}{2} + \frac{\sqrt{5}}{2}\right) - \frac{192}{5}\zeta(3) \right) \right] \right\} \\ & + a_1^M \left\{ \frac{1639L}{18} - 50964\zeta(5) + 12618\pi^2\zeta(3) + \frac{208846\zeta(3)}{5} - 324\pi^2 \ln(2) \right. \\ & + \frac{1163\pi^4}{120} - \frac{541129\pi^2}{36} + \frac{3604333}{1080} + n_l T_f \left(-\frac{22L}{3} - 4\pi^2 - \frac{80}{3} \right) \\ & + T_f \left(-\frac{22L}{3} + \frac{19532}{3} + 316\pi^2 - \frac{544\pi^4}{25} - \frac{29856}{5}\zeta(3) \right. \\ & \left. \left. - \frac{716}{5}\pi^2\sqrt{5} + \frac{2976}{5}\pi^2 \ln\left(\frac{1}{2} + \frac{\sqrt{5}}{2}\right) \right) \right. \\ & + i\pi \left[-\frac{149L}{3} + \frac{103\pi^2}{10} - \frac{5923}{36} + n_l T_f (4L + 14) + T_f \left(4L + 990 - \frac{576}{5}\zeta(3) \right. \right. \\ & \left. \left. - 1432\sqrt{5} \ln\left(\frac{1}{2} + \frac{\sqrt{5}}{2}\right) + 2976 \ln^2\left(\frac{1}{2} + \frac{\sqrt{5}}{2}\right) \right) \right] \left. \right\} \end{aligned}$$

$$\begin{aligned}
& + a_2^M \left\{ -\frac{1169L}{60} + 170274\zeta(5) - 42138\pi^2\zeta(3) - \frac{4896383\zeta(3)}{35} + \frac{2392}{3}\pi^2 \ln(2) \right. \\
& \quad - \frac{199\pi^4}{12} + \frac{13604203\pi^2}{270} - \frac{733820723}{75600} + n_l T_f \left(\frac{7L}{5} - 2\pi^2 + \frac{8059}{300} \right) \\
& \quad + T_f \left(\frac{7L}{5} - \frac{1585223}{900} - \frac{3322}{3}\pi^2 + \frac{1112}{25}\pi^4 + \frac{36288}{5}\zeta(3) \right. \\
& \quad \quad \left. + \frac{2768}{5}\pi^2\sqrt{5} - \frac{13248}{5}\pi^2 \ln\left(\frac{1}{2} + \frac{\sqrt{5}}{2}\right) \right) \\
& \quad + i\pi \left[\frac{953\pi^2}{210} - \frac{47929}{720} + \frac{6}{5} n_l T_f + T_f \left(-\frac{39182}{15} - \frac{1152}{5}\zeta(3) \right) \right. \\
& \quad \quad \left. + 5536\sqrt{5} \ln\left(\frac{1}{2} + \frac{\sqrt{5}}{2}\right) - 13248 \ln^2\left(\frac{1}{2} + \frac{\sqrt{5}}{2}\right) \right] \left. \right\}. \tag{43}
\end{aligned}$$

The corresponding charm-mass dependent part reads

$$\begin{aligned}
\Delta V_{11}^{(2)} \Big|_{m_c} &= \left\{ -\frac{4}{3}z^2 q_3(z) + 16z^2 \ln(z) q_4(z) + 24z^2 q_5(z) - \frac{2}{3}(22z + 1)q_6(z) \right. \\
& \quad + 18z(4z - 1)q_7(z) - 4\sqrt{z}(28z - 1)q_8(z) + 16z^2 q_{10}(z) + 2z^2 q_{11}(z) \\
& \quad - 16z^{3/2} q_{12}(z) + 92z - 2\pi^2 \left(23z^2 + 3z + \sqrt{z} - \frac{1}{3} \right) - 16\sqrt{z} \text{Li}_2(1 - \sqrt{z}) \\
& \quad + 2(3z^2 - 3z - 1) \ln^2(z) + 76z \ln(z) + 4(3z^2 - 3z + \sqrt{z} + 1) \text{Li}_2(1 - z) \\
& \quad + i\pi \left[24z^2(2 \ln(z) - 3) \ln^2(\eta) - 32z^2 q_1(z) + 296z \right. \\
& \quad \quad \left. - 4 \ln(z) + 4(22z + 1)q_2(z) \right] \left. \right\} \\
& + a_1^M \left\{ -288z^2 \ln^2(\eta) \text{Li}_2(\eta) - 4z^2 q_3(z) + 8z^2 (12z^2 + 16z + 3 + 6 \ln(z)) q_4(z) \right. \\
& \quad - \frac{2}{3} (72z^3 + 84z^2 + 22z + 1) q_6(z) - \frac{4}{15z} (45z^3 - 5z^2 + 3) \text{Li}_2(1 - z) \\
& \quad + \frac{2}{z} \left(36z^4 - 312z^3 + \frac{467}{3}z^2 - z + \frac{1}{5} \right) q_7(z) + 576z^3 - 336z^2 \\
& \quad - \frac{4}{3\sqrt{z}} \left(216z^4 - 504z^3 - 44z^2 - 32z + \frac{3}{5} \right) q_8(z) + \frac{18892}{3}z \\
& \quad + 8z(3z^3 - 8z^2 - 6z - 3) q_{10}(z) - 12z^2 q_{11}(z) + 112z^{3/2} q_{12}(z) \left. \right\}
\end{aligned}$$

$$\begin{aligned}
& + \frac{2}{15\sqrt{z}} (20z^2 + 20z + 3) (8\text{Li}_2(1 - \sqrt{z}) - 2\text{Li}_2(1 - z) + \pi^2) \\
& + \frac{2\pi^2}{15z} (2325z^3 + 5z^2 + 30z - 3) + 4z (144z^2 - 72z + 613) \ln(z) \\
& - \frac{2}{15z} (45z^3 - 5z^2 + 3) \ln^2(z) \\
& + i\pi \left[288z^3 + 24z^2 (12z^2 + 16z + 6 \ln(z) + 3) \ln^2(\eta) - 96z^2 q_1(z) + 360z^2 \right. \\
& \quad \left. + 328z - 4 \ln(z) + 4 (72z^3 + 84z^2 + 22z + 1) q_2(z) \right] \Big\} \\
& + a_2^M \left\{ -8z^2 (-3 \ln^2(\eta) - 12\text{Li}_2(\eta) + 2\pi^2)^2 \right. \\
& \quad - 16z^2 (40z^3 + 30z^2 - 6 \ln(z) - 1) q_4(z) - \frac{2}{3} \pi^2 z (1649z + 9) \\
& \quad + \frac{8}{3} z (120z^3 + 70z^2 - 11z - 6) q_6(z) + 6(z - 1)z (\ln^2(z) + 2\text{Li}_2(1 - z)) \\
& \quad - 2z (240z^3 - 330z^2 - 971z + 9) q_7(z) \\
& \quad + 16z^{3/2} (120z^3 - 185z^2 - 51z - 147) q_8(z) \\
& \quad - 4z^2 (40z^3 - 75z^2 + 11) q_{10}(z) + 42z^2 q_{11}(z) - 96z^{3/2} q_{12}(z) \\
& \quad - \frac{4}{3} z (2880z^3 - 1140z^2 - 823z - 54) \ln(z) \\
& \quad - \frac{2}{9} z (17280z^3 - 8280z^2 - 2861z + 1908) \\
& \quad \left. + i\pi \left[-48z^2 (40z^3 + 30z^2 - 6 \ln(z) - 1) \ln^2(\eta) - 192z^2 q_1(z) \right. \right. \\
& \quad \left. - \frac{8}{3} z (720z^3 + 480z^2 - 37z - 183) \right. \\
& \quad \left. \left. - 16z (120z^3 + 70z^2 - 11z - 6) q_2(z) \right] \right\}, \tag{44}
\end{aligned}$$

with $z \equiv m_c^2/m_b^2$. The variable η and the functions $q_i(z)$ are defined in Appendix B.2. One can check that $\Delta V_{11}^{(2)}|_{m_c}$ vanishes for $z \rightarrow 0$, and that for $z \rightarrow 1$ it approaches the corresponding contribution of a bottom quark contained in (43).

The case of $V_{12}^{(2)}$ is simpler since the corresponding one-loop expression vanishes due to the colour structure, and therefore one also has

$$\Delta V_{12}^{(2)}|_{m_c} = 0. \tag{45}$$

Hence there is no need to distinguish between the massive and massless charm contribution. We obtain

$$\begin{aligned}
V_{12}^{(2)} = & \left\{ 18L^2 + 156L + 3744\zeta(5) - 936\pi^2\zeta(3) - \frac{14833\zeta(3)}{5} + 72\pi^2 \ln(2) + \frac{239\pi^4}{90} \right. \\
& \left. + \frac{12487\pi^2}{12} + \frac{5347}{60} + i\pi \left[18L - 16\zeta(3) + \frac{47\pi^2}{45} + \frac{1333}{12} \right] \right\} \\
& + a_1^M \left\{ -33L - 19008\zeta(5) + 4752\pi^2\zeta(3) + \frac{77157\zeta(3)}{5} - 24\pi^2 \ln(2) - \frac{181\pi^4}{10} \right. \\
& \left. - \frac{21807\pi^2}{4} + \frac{4568}{15} + i\pi \left[18L + \frac{23\pi^2}{5} + \frac{15}{4} \right] \right\} \\
& + a_2^M \left\{ \frac{63L}{10} + 74304\zeta(5) - 18576\pi^2\zeta(3) - \frac{2236872\zeta(3)}{35} - 2064\pi^2 \ln(2) + \frac{797\pi^4}{10} \right. \\
& \left. + \frac{204218\pi^2}{9} + \frac{32369221}{12600} + i\pi \left[-\frac{18\pi^2}{35} - \frac{173}{30} \right] \right\}. \tag{46}
\end{aligned}$$

The integrated two-loop kernels for the colour-suppressed tree amplitude follow from (36), and read

$$\begin{aligned}
V_{21}^{(2)} &= -\frac{1}{3} V_{11}^{(2)} + \frac{4}{9} V_{12}^{(2)} - \frac{10}{3} n_l T_f - \frac{10}{3} T_f - \frac{49}{2}, \\
V_{22}^{(2)} &= 2 V_{11}^{(2)} + \frac{1}{3} V_{12}^{(2)} + 6 V_{11}^{(1)}. \tag{47}
\end{aligned}$$

Our results agree with those in [12, 13]. The comparison we performed is of analytic nature, except for those contributions to the real part of the amplitudes that stem from charm and bottom loop insertions into a gluon propagator, for which the result has been obtained in [13] only in numerical form. For these terms the numerical agreement for the values of the quark masses covered in Table 1 of [13] with our analytic result is within three permille.

6 Phenomenological applications

6.1 Input parameters

In this section we begin the discussion of the numerical evaluation of the topological tree amplitudes α_1 , α_2 , and the tree-dominated charmless B decays into final states $\pi\pi$, $\pi\rho$, and $\rho\rho$. The main result of this work, the NNLO vertex correction, depends on very few input parameters: the strong coupling α_s via $\Lambda_{\overline{\text{MS}}}^{(5)}$; the bottom pole mass m_b or $\overline{\text{MS}}$ mass $\bar{m}_b(\bar{m}_b)$; the renormalization scale $\mu \equiv \mu_b$ (to distinguish it from the hard-collinear scale that appears in spectator scattering); the Gegenbauer moments of the light-meson light-cone distribution amplitude a_n^M , the only hadronic parameters; and the electroweak-scale

Parameter	Value/Range	Parameter	Value/Range
$\Lambda_{\overline{\text{MS}}}^{(5)}$	0.225	μ_{hc}	1.5 ± 0.6
m_c	1.3 ± 0.2	f_{B_d}	0.195 ± 0.015
$m_s(2 \text{ GeV})$	0.09 ± 0.02	f_π	0.131
$(m_u + m_d)/m_s$	0.0826	$f_+^{B\pi}(0)$	$0.25 \pm 0.05^\dagger$
m_b	4.8	f_ρ	0.209
$\bar{m}_b(\bar{m}_b)$	4.2	$A_0^{B\rho}(0)$	$0.30 \pm 0.05^\dagger$
$ V_{cb} $	0.0415 ± 0.0010	$\lambda_B(1 \text{ GeV})$	$0.35 \pm 0.15^\dagger$
$ V_{ub}/V_{cb} $	0.09 ± 0.02	$\sigma_1(1 \text{ GeV})$	1.5 ± 1
γ	$(70 \pm 10)^\circ$	$\sigma_2(1 \text{ GeV})$	3 ± 2
$\tau(B^-)$	1.64 ps	$a_2^\pi(2 \text{ GeV})$	0.2 ± 0.15
$\tau(B_d)$	1.53 ps	$a_2^\rho(2 \text{ GeV})$	0.1 ± 0.15
μ_b	$4.8_{-2.4}^{+4.8}$	$a_{2,\perp}^\rho(2 \text{ GeV})$	0.1 ± 0.15

[†] Value and range changed to $f_+^{B\pi}(0) = 0.23 \pm 0.03$, $A_0^{B\rho}(0) = 0.28 \pm 0.03$, $\lambda_B(1 \text{ GeV}) = (0.20_{-0.00}^{+0.05}) \text{ GeV}$ in parameter set ‘‘Theory II’’. See text in Section 6.4.

Table 1: List of input parameters. Dimensionful parameters are given in units of 1 GeV.

initial conditions for the Wilson coefficients of the effective Hamiltonian. Their values and uncertainties are specified in Table 1, except for the electroweak-scale parameters $M_W = 80.4 \text{ GeV}$, $\bar{m}_t(\bar{m}_t) = 167 \text{ GeV}$ and $\sin^2\theta_W = 0.23$. When we evaluate the full topological tree amplitudes and branching fractions including penguin amplitudes (using results from [9]), we need further Standard Model and hadronic parameters, which are also listed in the Table. The values and uncertainties follow [9, 51] with some minor adjustments that account for recent reevaluations or progress in error estimates of γ , f_B [52, 53], $A_0^{B\rho}(0)$ [54], and $a_{2,(\perp)}^\rho$ [55].

Together with the NNLO non-leptonic matrix elements, we now use three-loop evolution of the strong coupling, as well as the next-to-next-to-leading-logarithmic (NNLL) approximation to the Wilson coefficients appearing in the effective weak interaction Hamiltonian in the CMM basis. This approximation is constructed from the two-loop initial conditions [45, 56], three-loop anomalous dimension matrix [44, 45] and the NNLL solution to the renormalization group equation [57]. The penguin amplitudes, which are not yet known at NNLO, are evaluated exactly as in [9], whenever needed, except that we employ the same three-loop evolved strong coupling in the entire numerical program. The observables we discuss in this paper are chosen such that they do not depend

significantly on the penguin amplitudes.

6.2 Topological tree amplitudes at NNLO

6.2.1 Two-loop vertex correction

We first consider the loop expansion of the pieces of the topological tree amplitudes not related to spectator scattering, as defined in (37). To acquire an idea of the convergence of the perturbative expansion we provide a numerical representation of

$$\int_0^1 du T_j(u) \phi_M(u) = V_{1j}^{(0)} + \sum_{l \geq 1} \left(\frac{\alpha_s}{4\pi} \right)^l \frac{C_F}{2N_c} V_{1j}^{(l)} \quad (48)$$

up to $\mathcal{O}(\alpha_s^2)$, and similarly for $\tilde{T}_j(u)$ and $V_{2j}^{(l)}$. Choosing $\mu = m_b$ we get

$$\begin{aligned} \int_0^1 du T_1(u) \phi_M(u) &= 0 + [-5 - 2.094 i + (1.222 - 2.094 i) a_1^M - 0.233 a_2^M] \left(\frac{\alpha_s}{4\pi} \right) \\ &\quad + [-38.510 - 75.389 i + (142.014 - 24.416 i) a_1^M \\ &\quad + (-18.588 - 13.528 i) a_2^M + \Delta_{m_c}] \left(\frac{\alpha_s}{4\pi} \right)^2, \\ \int_0^1 du T_2(u) \phi_M(u) &= 1 + [71.598 + 71.320 i + (-47.327 + 34.313 i) a_1^M \\ &\quad + (0.848 - 7.569 i) a_2^M] \left(\frac{\alpha_s}{4\pi} \right)^2, \\ \int_0^1 du \tilde{T}_1(u) \phi_M(u) &= \frac{4}{9} + [0.333 + 0.698 i + (-0.407 + 0.698 i) a_1^M + 0.078 a_2^M] \left(\frac{\alpha_s}{4\pi} \right) \\ &\quad + \left[37.362 + 56.828 i + (-68.372 + 23.389 i) a_1^M \right. \\ &\quad \left. + (6.573 + 1.145 i) a_2^M - \frac{1}{3} \Delta_{m_c} \right] \left(\frac{\alpha_s}{4\pi} \right)^2, \\ \int_0^1 du \tilde{T}_2(u) \phi_M(u) &= \frac{1}{3} + [-10 - 4.189 i + (2.444 - 4.189 i) a_1^M - 0.467 a_2^M] \left(\frac{\alpha_s}{4\pi} \right) \\ &\quad + [-83.154 - 139.571 i + (275.585 - 49.960 i) a_1^M \\ &\quad + (-38.293 - 29.580 i) a_2^M + 2 \Delta_{m_c}] \left(\frac{\alpha_s}{4\pi} \right)^2. \end{aligned} \quad (49)$$

We observe that the NNLO terms have relatively large coefficients, but since $\alpha_s(m_b) \approx 0.22$, the perturbative expansion is still under control for most of the terms. The coefficients of the second Gegenbauer moment are generally rather small, contrary to those of the first one, as we will discuss in more detail at the end of this subsection.

The numbers in (49) apply when we treat the charm quark as massless. The charm mass effect, the difference between the contribution of a quark of mass m_c and that of a massless quark, is parameterized by Δ_{m_c} , for which we find the fitting formula

$$\begin{aligned}
\Delta_{m_c} = & -0.9661 - 2.0849 i - (11.4437 + 12.9458 i)(z - 0.075) \\
& + (28.0366 + 64.7300 i)(z - 0.075)^2 \\
& + [4.5919 - 1.9379 i + (14.4270 - 12.2979 i)(z - 0.075) \\
& - (96.8420 - 59.5511 i)(z - 0.075)^2] a_1^M \\
& + [-0.3599 - 0.3833 i - (2.2574 + 0.5738 i)(z - 0.075) \\
& + (14.1412 + 7.0945 i)(z - 0.075)^2] a_2^M
\end{aligned} \tag{50}$$

in the region of $z = m_c^2/m_b^2$ of interest. The second-order polynomials in z were obtained from a least-squares fit to the exact functions, which works better than 0.4% for $z \in [0.05, 0.10]$. The size of the charm-mass dependent terms is moderate. Most of the numbers in (49) receive small corrections, but the shifts induced by the z -dependent terms can be up to 11% for single entries.

The successive LO, NLO and NNLO approximations⁵ to the topological tree amplitude parameters $\alpha_1(\pi\pi)$ and $\alpha_2(\pi\pi)$ (vertex correction only, i.e. no spectator scattering) are shown in Figure 3, depending on the renormalization scale μ . Relative to the NLO correction the NNLO term turns out to be sizeable. For the colour-allowed amplitude $\alpha_1(\pi\pi)$ this can be explained by the observation that the NLO correction is colour-suppressed, while the NNLO correction is no longer colour-suppressed for any of the two amplitudes. As in any perturbative QCD calculation the higher-order corrections are expected to reduce the scale uncertainties compared to lower-order approximations. We observe that this is indeed the case after taking into account the NNLO corrections for the real parts of the amplitudes, but the reduction is absent for the imaginary parts. We attribute this to the fact that the two-loop contribution to the imaginary part is really a next-to-leading order effect since the imaginary part is zero at tree-level, and to the large size of the two-loop correction.

Besides the renormalization scale the vertex correction to the topological tree amplitudes depends only on the Gegenbauer moments. At leading order there is no dependence on these moments, whereas at NLO this dependence is given by

$$\begin{aligned}
[\alpha_1]_V &= 1.040 + 0.013i - (0.007 - 0.013i) a_1^{M_2} + 0.001 a_2^{M_2}, \\
[\alpha_2]_V &= 0.029 - 0.079i + (0.046 - 0.079i) a_1^{M_2} - 0.009 a_2^{M_2},
\end{aligned} \tag{51}$$

⁵The LO and NLO result is computed in the traditional operator basis for the effective weak Hamiltonian, so that it corresponds to the expressions used in [1, 3], but is slightly different from the NLO truncations of the NNLO results of the present calculation.

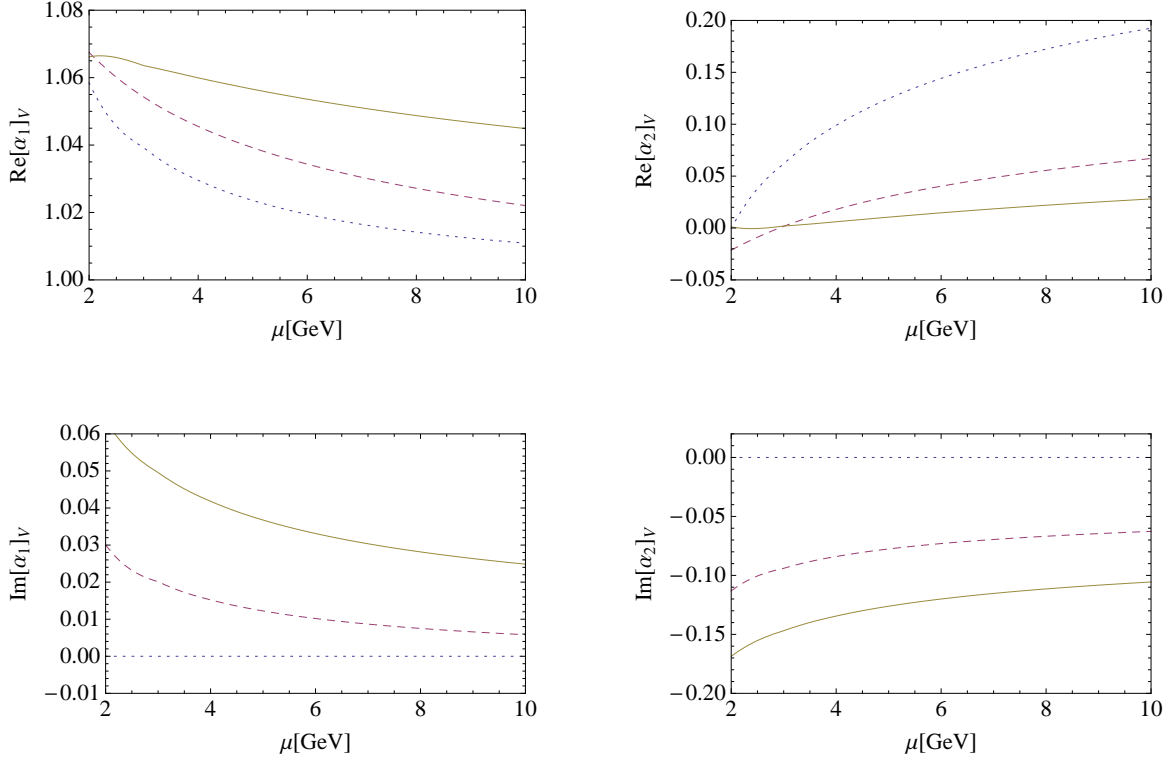


Figure 3: Dependence of the topological tree amplitudes $\alpha_1(\pi\pi)$ and $\alpha_2(\pi\pi)$ on the hard scale μ (vertex corrections only). The dotted, dashed and solid lines refer to the theoretical predictions at LO, NLO and NNLO, respectively.

where we choose again $\mu = m_b$. At NNLO we obtain

$$\begin{aligned}
[\alpha_1]_V &= 1.057 + 0.038i - (0.032 - 0.022i) a_1^{M_2} + (0.003 - 0.001i) a_2^{M_2}, \\
[\alpha_2]_V &= 0.013 - 0.126i + (0.139 - 0.096i) a_1^{M_2} - (0.021 + 0.009i) a_2^{M_2}.
\end{aligned} \tag{52}$$

Since the Gegenbauer moments are typically smaller than 0.3, we conclude that the dependence on the second moment $a_2^{M_2}$ is very small for both tree amplitudes. This implies that there is practically no dependence on the shape of the pion or rho meson light-cone distribution amplitude in the vertex term of the factorization formula (1). This is no longer true once spectator scattering is included, especially for the colour-suppressed tree amplitude α_2 , as discussed in [6]. The first Gegenbauer moment is more important and has a significant effect on the value of the colour-suppressed amplitude $[\alpha_2]_V$, which is furthermore enhanced at NNLO. This is a source of non-factorizable SU(3) flavour symmetry breaking (not related to decay constants and heavy-to-light form factors) in the relation of amplitudes with pions and kaons.

6.2.2 Complete NNLO amplitude including spectator scattering

We now proceed with our investigation of the topological tree amplitudes by adding the corrections from spectator scattering on top of those from the vertex corrections. Our numerical results for the $\pi\pi$ final states read

$$\begin{aligned}\alpha_1(\pi\pi) &= 1.009 + [0.023 + 0.010 i]_{\text{NLO}} + [0.026 + 0.028 i]_{\text{NNLO}} \\ &\quad - \left[\frac{r_{\text{sp}}}{0.445} \right] \left\{ [0.014]_{\text{LOsp}} + [0.034 + 0.027 i]_{\text{NLOsp}} + [0.008]_{\text{tw3}} \right\} \\ &= 1.000^{+0.029}_{-0.069} + (0.011^{+0.023}_{-0.050})i,\end{aligned}\tag{53}$$

$$\begin{aligned}\alpha_2(\pi\pi) &= 0.220 - [0.179 + 0.077 i]_{\text{NLO}} - [0.031 + 0.050 i]_{\text{NNLO}} \\ &\quad + \left[\frac{r_{\text{sp}}}{0.445} \right] \left\{ [0.114]_{\text{LOsp}} + [0.049 + 0.051 i]_{\text{NLOsp}} + [0.067]_{\text{tw3}} \right\} \\ &= 0.240^{+0.217}_{-0.125} + (-0.077^{+0.115}_{-0.078})i.\end{aligned}\tag{54}$$

Here the “NNLO” term in the first line of each of the two equations corresponds to the numerical evaluation of the calculation of this paper, while the second line accounts for spectator scattering at $\mathcal{O}(\alpha_s)$ (“LOsp”) and $\mathcal{O}(\alpha_s^2)$ (“NLOsp”) and a certain power correction (“tw3”). The theoretical calculation for spectator scattering is taken from [6], but the numerical values differ, since we now use a different operator basis, which redistributes the perturbative expansion, and slightly different input parameters. The third line sums all contributions and provides an estimate of the theoretical uncertainties from the parameter variations detailed in Table 1. By comparing the theoretical uncertainty in the full expressions above to the one from the vertex correction alone, see Figure 3, we see that it arises primarily from spectator scattering. The main contributors to the uncertainty are the parameter combination

$$r_{\text{sp}} = \frac{9f_\pi \hat{f}_B}{m_b f_+^{B\pi}(0) \lambda_B},\tag{55}$$

which appears as an overall normalization factor of the spectator-scattering term, the second Gegenbauer moment $a_2^\pi(2\text{ GeV})$, and “tw3” power correction.

Relative to the full amplitude the two-loop vertex correction is only a few percent for the colour-allowed amplitude α_1 , but it is quite significant for α_2 . The negative (10 – 15)% correction to the real part decreases the branching fractions of the colour-suppressed decays by about 25% relative to previous results that included the $\mathcal{O}(\alpha_s^2)$ correction only in spectator scattering. The magnitude of the correction to the imaginary part of α_2 at two loops still reaches 25% of the leading-order real part. However, we also observe that the two $\mathcal{O}(\alpha_s^2)$ corrections, “NNLO” in the vertex term and “NLOsp” in spectator scattering, cancel to a large extent in both, their real and imaginary parts. This is somewhat unfortunate, since an enhancement rather than a cancellation in the colour-suppressed tree amplitude might have been welcome in view of the trend indicated by experimental data, as will be seen below.

The colour-suppressed tree amplitude $\alpha_2(\pi\pi)$ exhibits an interesting structure. It starts out with a positive real value 0.220 that corresponds to the naive factorization approximation. After adding the perturbative corrections to the four-quark vertex (the first line of (54)), it is found to be almost purely imaginary, $0.01 - 0.13i$. However, the spectator-scattering mechanism regenerates a real part of roughly the original size and cancels part of the strong phase. The net result of this is that the colour-suppressed tree amplitude can become sizeable in QCD factorization when r_{sp} is large, but since this enhances the cancellation of the imaginary part, one cannot have both, a large magnitude and a large strong phase. In comparison, the colour-allowed tree amplitude $\alpha_1(\pi\pi)$ is rather stable against radiative corrections, and never deviates by a large amount from its naive-factorization estimate.

6.3 Parameter dependence of branching fraction ratios

6.3.1 Factorization test

In this subsection we consider a non-leptonic to semi-leptonic decay ratio that provides direct access to the magnitude of the topological tree amplitudes. This analysis has first been performed in [5] at NLO and can now be repeated at NNLO, and with improved experimental data (see also [15]).

Within the approximation that all electroweak contributions are neglected since they are never CKM-enhanced and formally of order $\mathcal{O}(\alpha_{em})$, the process $B^- \rightarrow \pi^- \pi^0$ is a pure tree decay. The corresponding decay amplitude in the SM can be written as [5]

$$\sqrt{2} \mathcal{A}_{B^- \rightarrow \pi^- \pi^0} = A_{\pi\pi} \sum_{p=u,c} \lambda_p^d \delta_{pu} (\alpha_1 + \alpha_2), \quad (56)$$

with $A_{\pi\pi} = i \frac{G_F}{\sqrt{2}} m_B^2 f_+^{B\pi}(0) f_\pi$, and $\lambda_p^d = V_{pb} V_{pd}^*$. A substantial uncertainty in the prediction of the branching ratio arises from the overall normalization due to $|V_{ub}|$ and $f_+^{B\pi}(0)$. These two quantities cancel out in the ratio [5, 58]

$$R_\pi \equiv \frac{\Gamma(B^- \rightarrow \pi^- \pi^0)}{d\Gamma(\bar{B}^0 \rightarrow \pi^+ l^- \bar{\nu})/dq^2|_{q^2=0}} = 3\pi^2 f_\pi^2 |V_{ud}|^2 |\alpha_1(\pi\pi) + \alpha_2(\pi\pi)|^2, \quad (57)$$

and a direct measurement of the tree amplitude coefficients can be performed if the differential semi-leptonic $B \rightarrow \pi l \nu$ rate is measured near $q^2 = 0$. The ratio R_π in (57) therefore constitutes a test of QCD factorization, and furthermore underlines the importance of measuring the semi-leptonic decay spectrum for understanding the pattern of non-leptonic B decays. Replacing pions by longitudinally polarized rho mesons in (57), we define an analogous ratio R_ρ , which allows us to test factorization in $B \rightarrow VV$ decays.

This test can currently be carried out for pions. The latest experimental data on the $B^- \rightarrow \pi^- \pi^0$ branching fraction reads [59–62]

$$\text{Br}(B^- \rightarrow \pi^- \pi^0) = (5.59_{-0.40}^{+0.41}) \cdot 10^{-6}. \quad (58)$$

Since the theoretical expression for the differential semi-leptonic spectrum at the end-point assumes the form

$$d\Gamma(\bar{B}^0 \rightarrow \pi^+ l^- \bar{\nu})/dq^2|_{q^2=0} = \frac{G_F^2 m_B^3}{192 \pi^3} \left[|V_{ub}| f_+^{B\pi}(0) \right]^2, \quad (59)$$

the measurement of the left-hand side is equivalent to the experimental determination of $|V_{ub}| f_+^{B\pi}(0)$ from the full lepton invariant mass spectrum in $B \rightarrow \pi l \nu$ decay together with an extrapolation to $q^2 = 0$ based on a form-factor parameterization. Several extractions of $|V_{ub}| f_+^{B\pi}(0)$ [63–65] employing different parameterizations of the transition form factor [66–69] can be found in the literature, which all yield similar results. We shall adopt the value

$$|V_{ub}| f_+^{B\pi}(0) = (9.1 \pm 0.7) \cdot 10^{-4}. \quad (60)$$

Combining this and the experimental data on $\text{Br}(B^- \rightarrow \pi^- \pi^0)$ given by (58) allows us to extract the following experimental constraint on R_π ,

$$[R_\pi]_{\text{exp}} = 0.81 \pm 0.14, \quad (61)$$

which can be translated into a constraint on the tree amplitudes,

$$[|\alpha_1(\pi\pi) + \alpha_2(\pi\pi)|]_{\text{exp}} = 1.29 \pm 0.11. \quad (62)$$

On the other hand, varying the parameters in the range specified in Table 1 and adding the errors in quadrature, our theoretical prediction at NNLO is given by

$$|\alpha_1(\pi\pi) + \alpha_2(\pi\pi)| = 1.24_{-0.10}^{+0.16}, \quad (63)$$

which is in good agreement with the experimental data and hence provides support for the factorization assumption. The theoretical uncertainty is still large, but much of it arises from λ_B , \hat{f}_B and $f_+^{B\pi}(0)$, on which the theoretical result depends only through the overall factor r_{sp} in (55). In Figure 4 we therefore plot the dependence of $|\alpha_1(\pi\pi) + \alpha_2(\pi\pi)|$ on the first inverse moment of the B -meson distribution amplitude, λ_B , and the remaining theoretical error (grey band). For comparison we show the LO (flat, dotted line), NLO (dashed) and NNLO calculation, which makes it clear that the combined NNLO correction is rather small. The overlaid horizontal band refers to the experimental value (62), displaying again the good agreement with the theoretical calculation. The errors are too large to turn this into a determination of the parameter λ_B , which may then serve as an input for the remaining non-leptonic observables. The central experimental value (thick horizontal line) alone would allow the range $\lambda_B \in [150, 400]$ MeV, which is on the lower side of theoretical expectations [1, 3, 70–72].

In the future it should be of interest to extend the factorization test to other final states. In Table 2 we summarize our predictions for pions and longitudinal rho mesons. Here “Theory I” corresponds to the input parameters of Table 1. As will become clear below, the analysis of non-leptonic decay data suggests the hypothesis of smaller form factors and λ_B . This leads us to choose a second parameter set, to be discussed in Section 6.4 and labelled “Theory II”. We consider the corresponding entries in Table 2 to be our reference predictions.

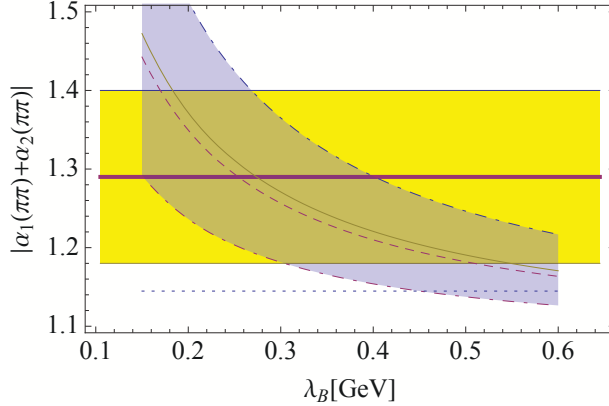


Figure 4: Dependence of the theoretical prediction of $|\alpha_1(\pi\pi) + \alpha_2(\pi\pi)|$ (equivalent to R_π) on λ_B and comparison to $[|\alpha_1(\pi\pi) + \alpha_2(\pi\pi)|]_{\text{exp}} = 1.29 \pm 0.11$. The dotted, dashed and solid lines denote the LO, NLO and NNLO predictions, respectively. The dot-dashed lines give the error band upon varying the input parameters within the ranges specified in Table 1, excluding the parameters contained in r_{sp} . The experimental data within 1σ error is also shown (horizontal band).

6.3.2 Ratios involving the colour-suppressed tree amplitude

Next we consider a number of branching fraction ratios to further highlight the importance of hard spectator-scattering, and thereby the dependence on λ_B and r_{sp} . Some of these ratios have been considered before, for instance in [5, 15, 73], for a different purpose. We define

$$\begin{aligned}
 R_{+-}^{\pi\pi} &\equiv 2 \frac{\Gamma(B^- \rightarrow \pi^- \pi^0)}{\Gamma(B^0 \rightarrow \pi^+ \pi^-)}, & R_{00}^{\pi\pi} &\equiv 2 \frac{\Gamma(B^0 \rightarrow \pi^0 \pi^0)}{\Gamma(B^0 \rightarrow \pi^+ \pi^-)}, \\
 R_{+-}^{\rho\rho} &\equiv 2 \frac{\Gamma(B^- \rightarrow \rho_L^- \rho_L^0)}{\Gamma(B^0 \rightarrow \rho_L^+ \rho_L^-)}, & R_{00}^{\rho\rho} &\equiv 2 \frac{\Gamma(B^0 \rightarrow \rho_L^0 \rho_L^0)}{\Gamma(B^0 \rightarrow \rho_L^+ \rho_L^-)}, \\
 R_{00}^{\pi\rho} &\equiv \frac{2 \Gamma(B^0 \rightarrow \pi^0 \rho^0)}{\Gamma(B^0 \rightarrow \pi^+ \rho^-) + \Gamma(B^0 \rightarrow \pi^- \rho^+)}.
 \end{aligned} \tag{64}$$

	Theory I	Theory II	Experiment
R_π	$0.75^{+0.20}_{-0.11}$	$0.94^{+0.23}_{-0.22}$	0.81 ± 0.14
R_ρ	$1.75^{+0.37}_{-0.24}$	$2.08^{+0.50}_{-0.46}$	—

Table 2: Theoretical results for the factorization test ratios (57) for pions and longitudinal rho mesons. “Theory II” refers to our preferred input parameter set, see text.

Here, and throughout the paper, Γ denotes the CP-averaged decay rate, i.e. $\Gamma(B \rightarrow f)$ is in fact the average of $\Gamma(B \rightarrow f)$ and the decay rate $\Gamma(\bar{B} \rightarrow \bar{f})$ of the CP-conjugate mode. The R_{00} ratios are approximately proportional to the square of the ratio of the colour-suppressed to the colour-allowed tree amplitude. This approximation is very good for the modes involving the rho meson final states, where the penguin contribution is known to be small.⁶ The R_{+-} ratios involve $|\alpha_1 + \alpha_2|$, similar to R_π and R_ρ in the previous subsection, but divided by $|\alpha_1|$ and squared. These ratios also display some sensitivity to the CKM angle γ for $\pi\pi$, but we do not discuss this here, since it arises through interference with the penguin amplitudes.

Our results for these ratios are displayed in Figure 5. Again the grey band refers to the theoretical prediction (with uncertainty) for the value of λ_B on the horizontal axis, while the horizontal band gives the current measurement [59–62, 74–88]. It is clear that naive factorization (the dotted line) fails to describe the data. In general, QCD factorization provides a good description of data, especially if λ_B is around 200 MeV, where, however, the theoretical uncertainty becomes large. In the QCD factorization approach small λ_B and a large colour-suppressed amplitude is connected with an important role of spectator scattering in the dynamics underlying this amplitude as already noted in [5]. An exception to the good agreement between theory and data is $R_{00}^{\pi\pi}$ which can be accommodated even for $\lambda_B \simeq 200$ MeV only marginally within errors. Thus, it is plausible or even likely that power-suppressed corrections are also important for the colour-suppressed amplitude, especially if it is accompanied by a large phase, an issue that we do not discuss in the present paper, since it requires the consideration of penguin amplitudes. Explaining why this effect should be large for pions but small for rho mesons (rather than fitting it with new parameters [89, 90]) appears to be a theoretical challenge.

6.3.3 Ratios involving other $\pi\rho$ final states

Next we discuss two ratios that involve only the charged $\pi^\pm\rho^\mp$ final states. These final states are dominated by the two colour-allowed tree amplitudes $\alpha_1(\pi\rho)$ and $\alpha_1(\rho\pi)$. The ratios we consider have few theoretical uncertainties other than the one from the heavy-to-light form factors [5]. Specifically, we define

$$R_3 \equiv \frac{\Gamma(\bar{B}^0 \rightarrow \pi^+\rho^-)}{\Gamma(\bar{B}^0 \rightarrow \pi^-\rho^+)}, \quad \Delta C \equiv \frac{1}{2} [C(\pi^-\rho^+) - C(\pi^+\rho^-)] , \quad (65)$$

where $C(f)$ denotes the coefficient of the $\cos(\Delta m_B t)$ term in the time-dependent decay amplitude into the final state f , see [5] for the relevant definitions. The dependence of the theoretical calculation on the form factor ratio $F_{\pi\rho} = A_0^{B\rho}(0)/f_+^{B\pi}(0)$ is shown in Figure 6 together with the present experimental data [59, 86–88, 91, 92]. The agreement

⁶For the vector-vector final state, we consider the longitudinally polarized final state. Accordingly, the experimental unpolarized branching fraction is multiplied by the measured longitudinal polarization fraction.

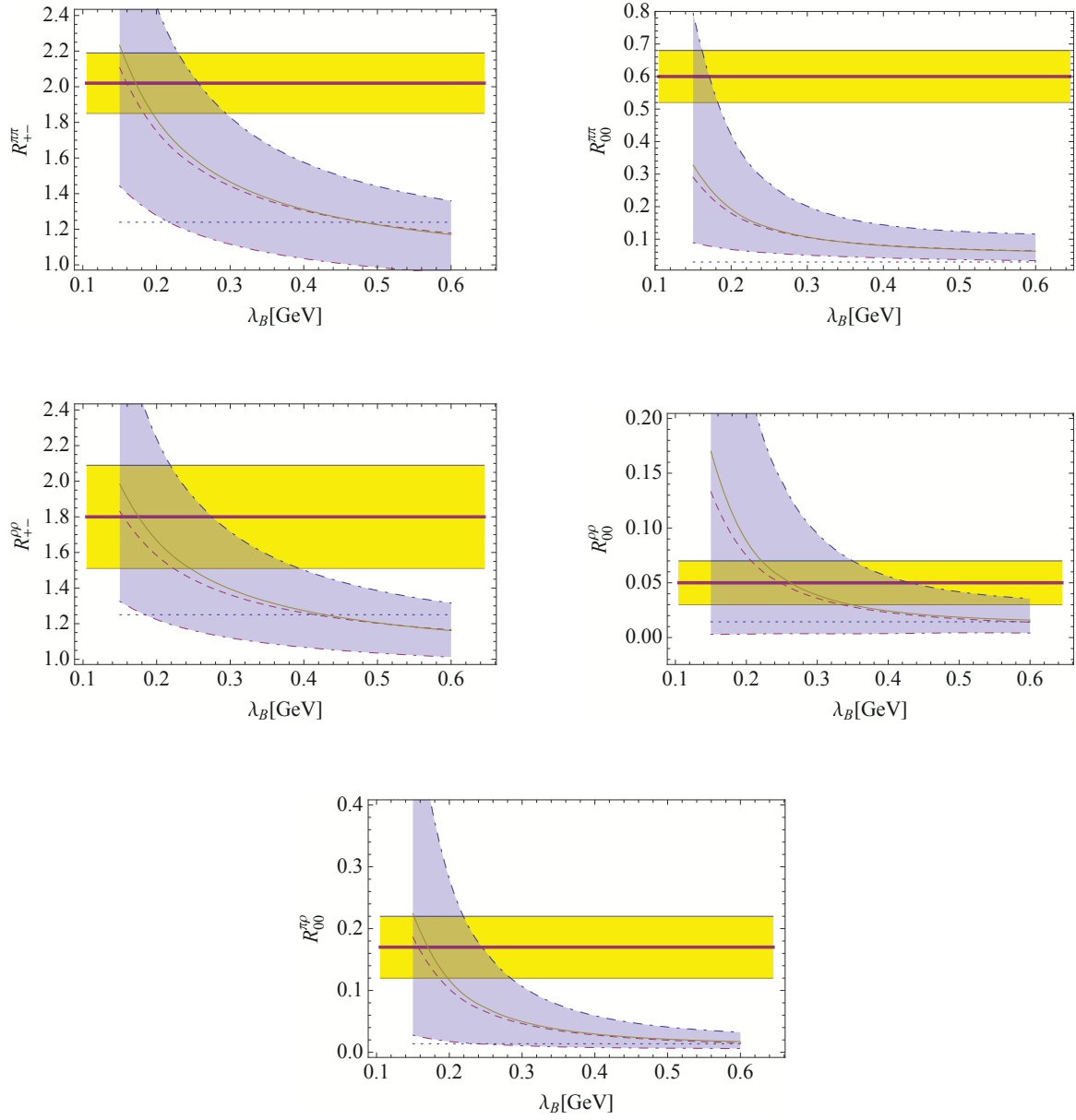


Figure 5: Constraints on λ_B from the ratios (64) of $B \rightarrow \pi\pi$, $B \rightarrow \pi\rho$, and $B \rightarrow \rho_L\rho_L$ decays. Line styles have the same meaning as in Figure 4.

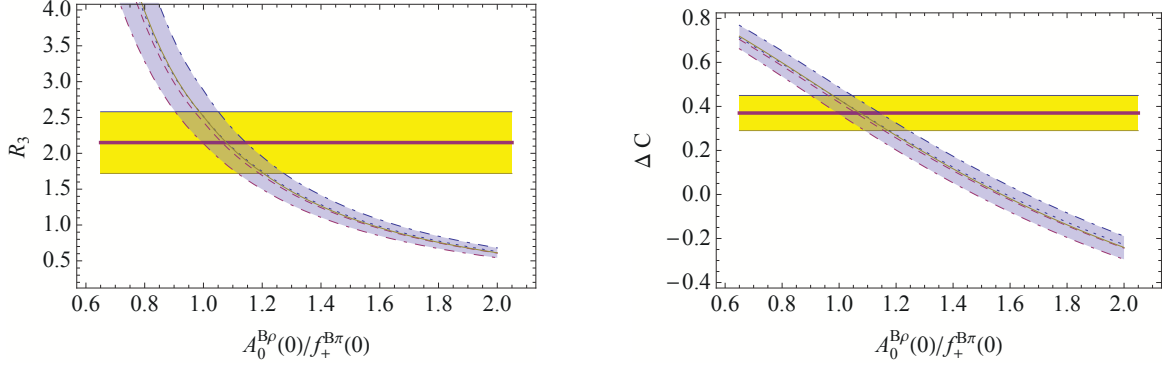


Figure 6: Dependence of R_3 and ΔC on the ratio $A_0^{B\rho}(0)/f_+^{B\pi}(0)$ of B -meson form factors for fixed $f_+^{B\pi}(0) = 0.25$. Our default input value for the form factor ratio is 1.20. Lines and bands have the same meaning as in Figure 4.

is excellent for $F_{\pi\rho} \in [1.0, 1.2]$, which is consistent with the input value 1.2 that follows from Table 1.

6.4 Final results

In this subsection we give our final theoretical predictions for the CP-averaged branching fractions and a number of ratios of CP-averaged $\pi\pi$, $\pi\rho$ and $\rho_L\rho_L$ decay rates. In addition to the ones already discussed in the previous subsections, we further consider the ratios

$$\begin{aligned}
 R_1 &\equiv \frac{\Gamma(\bar{B}^0 \rightarrow \pi^+\rho^-)}{\Gamma(\bar{B}^0 \rightarrow \pi^+\pi^-)}, & R_2 &\equiv \frac{\Gamma(\bar{B}^0 \rightarrow \pi^+\rho^-) + \Gamma(\bar{B}^0 \rightarrow \pi^-\rho^+)}{2\Gamma(\bar{B}^0 \rightarrow \pi^+\pi^-)}, \\
 R_4 &\equiv \frac{2\Gamma(B^- \rightarrow \pi^-\rho^0)}{\Gamma(\bar{B}^0 \rightarrow \pi^-\rho^+)} - 1, & & \\
 R_5 &\equiv \frac{2\Gamma(B^- \rightarrow \pi^0\rho^-)}{\Gamma(\bar{B}^0 \rightarrow \pi^+\rho^-)} - 1, & R_6 &\equiv \frac{\Gamma(\bar{B}^0 \rightarrow \pi^+\rho^-) + \Gamma(\bar{B}^0 \rightarrow \pi^-\rho^+)}{2\Gamma(\bar{B}^0 \rightarrow \rho_L^+\rho_L^-)}.
 \end{aligned} \tag{66}$$

R_3 has already been defined in (65). Moreover, we define the following ratios of the colour-suppressed decays,

$$R_C^\pi = \frac{\Gamma(\bar{B}^0 \rightarrow \pi^0\pi^0)}{\Gamma(\bar{B}^0 \rightarrow \pi^0\rho^0)}, \quad R_C^\rho = \frac{\Gamma(\bar{B}^0 \rightarrow \rho_L^0\rho_L^0)}{\Gamma(\bar{B}^0 \rightarrow \pi^0\rho^0)}, \tag{67}$$

to eliminate the input parameter correlations among the three decay modes.

The theoretical results and experimental measurements of the CP-averaged branching fractions of the twelve final states composed of pions and rho mesons, as well their ratios as defined above are summarized in Table 3. The column labelled ‘‘Theory I’’, on which we focus first, uses the input values and uncertainties defined in Table 1. The first error comprises the uncertainties from CKM parameters (γ , $|V_{cb}|$, $|V_{ub}|$ – see below), the

	Theory I	Theory II	Experiment
$B^- \rightarrow \pi^- \pi^0$	$5.43^{+0.06+1.45}_{-0.06-0.84}$ (★)	$5.82^{+0.07+1.42}_{-0.06-1.35}$ (★)	$5.59^{+0.41}_{-0.40}$
$\bar{B}_d^0 \rightarrow \pi^+ \pi^-$	$7.37^{+0.86+1.22}_{-0.69-0.97}$ (★)	$5.70^{+0.70+1.16}_{-0.55-0.97}$ (★)	5.16 ± 0.22
$\bar{B}_d^0 \rightarrow \pi^0 \pi^0$	$0.33^{+0.11+0.42}_{-0.08-0.17}$	$0.63^{+0.12+0.64}_{-0.10-0.42}$	1.55 ± 0.19
$B^- \rightarrow \pi^- \rho^0$	$8.68^{+0.42+2.71}_{-0.41-1.56}$ (★★)	$9.84^{+0.41+2.54}_{-0.40-2.52}$ (★★)	$8.3^{+1.2}_{-1.3}$
$B^- \rightarrow \pi^0 \rho^-$	$12.38^{+0.90+2.18}_{-0.77-1.41}$ (★)	$12.13^{+0.85+2.23}_{-0.73-2.17}$ (★)	$10.9^{+1.4}_{-1.5}$
$\bar{B}^0 \rightarrow \pi^+ \rho^-$	$17.80^{+0.62+1.76}_{-0.56-2.10}$ (★)	$13.76^{+0.49+1.77}_{-0.44-2.18}$ (★)	15.7 ± 1.8
$\bar{B}^0 \rightarrow \pi^- \rho^+$	$10.28^{+0.39+1.37}_{-0.39-1.42}$ (★★)	$8.14^{+0.34+1.35}_{-0.33-1.49}$ (★★)	7.3 ± 1.2
$\bar{B}^0 \rightarrow \pi^\pm \rho^\mp$	$28.08^{+0.27+3.82}_{-0.19-3.50}$ (†)	$21.90^{+0.20+3.06}_{-0.12-3.55}$ (†)	23.0 ± 2.3
$\bar{B}^0 \rightarrow \pi^0 \rho^0$	$0.52^{+0.04+1.11}_{-0.03-0.43}$	$1.49^{+0.07+1.77}_{-0.07-1.29}$	2.0 ± 0.5
$B^- \rightarrow \rho_L^- \rho_L^0$	$18.42^{+0.23+3.92}_{-0.21-2.55}$ (★★)	$19.06^{+0.24+4.59}_{-0.22-4.22}$ (★★)	$22.8^{+1.8}_{-1.9}$
$\bar{B}_d^0 \rightarrow \rho_L^+ \rho_L^-$	$25.98^{+0.85+2.93}_{-0.77-3.43}$ (★★)	$20.66^{+0.68+2.99}_{-0.62-3.75}$ (★★)	$23.7^{+3.1}_{-3.2}$
$\bar{B}_d^0 \rightarrow \rho_L^0 \rho_L^0$	$0.39^{+0.03+0.83}_{-0.03-0.36}$	$1.05^{+0.05+1.62}_{-0.04-1.04}$	$0.55^{+0.22}_{-0.24}$
$R_{+-}^{\pi\pi}$	$1.38^{+0.12+0.53}_{-0.13-0.32}$	$1.91^{+0.18+0.72}_{-0.20-0.64}$	2.02 ± 0.17
$R_{00}^{\pi\pi}$	$0.09^{+0.03+0.12}_{-0.02-0.04}$	$0.22^{+0.06+0.28}_{-0.05-0.16}$	0.60 ± 0.08
$R_{+-}^{\rho\rho}$	$1.32^{+0.02+0.44}_{-0.03-0.27}$	$1.72^{+0.03+0.64}_{-0.03-0.53}$	$1.80^{+0.28}_{-0.29}$
$R_{00}^{\rho\rho}$	$0.03^{+0.00+0.07}_{-0.00-0.03}$	$0.10^{+0.01+0.19}_{-0.01-0.11}$	0.05 ± 0.02
$R_{00}^{\pi\rho}$	$0.04^{+0.00+0.09}_{-0.00-0.03}$	$0.14^{+0.01+0.20}_{-0.01-0.13}$	0.17 ± 0.05
R_1	$2.41^{+0.16+0.32}_{-0.18-0.37}$	$2.41^{+0.17+0.37}_{-0.20-0.43}$	3.04 ± 0.37
R_2	$1.90^{+0.18+0.53}_{-0.19-0.41}$	$1.92^{+0.19+0.42}_{-0.20-0.40}$	2.23 ± 0.24
R_3	$1.73^{+0.13+1.12}_{-0.12-0.82}$	$1.69^{+0.13+0.72}_{-0.12-0.59}$	2.15 ± 0.43
R_4	$0.58^{+0.02+0.67}_{-0.02-0.35}$	$1.26^{+0.00+0.84}_{-0.00-0.75}$	$1.12^{+0.46}_{-0.48}$
R_5	$0.30^{+0.05+0.36}_{-0.04-0.20}$	$0.64^{+0.06+0.50}_{-0.05-0.41}$	$0.30^{+0.22}_{-0.23}$
R_6	$0.54^{+0.01+0.23}_{-0.01-0.17}$	$0.53^{+0.01+0.16}_{-0.01-0.13}$	0.49 ± 0.08
R_C^π	$0.64^{+0.22+0.64}_{-0.17-0.37}$	$0.42^{+0.09+0.28}_{-0.08-0.16}$	0.78 ± 0.22
R_C^ρ	$0.74^{+0.10+0.58}_{-0.09-0.46}$	$0.70^{+0.06+0.46}_{-0.06-0.39}$	$0.27^{+0.13}_{-0.14}$

Table 3: CP-averaged branching fractions in units of 10^{-6} [59–62, 74–88, 93–96] and various ratios of tree-dominated $B \rightarrow \pi\pi$, $\pi\rho$ and $\rho_L\rho_L$ decays. The first error on a quantity comes from the CKM parameters, while the second one stems from all other parameters added in quadrature [51]. We consider “Theory II” as our reference values, see text.

second combines all other uncertainties (scale, hadronic parameters, power correction parameters) in quadrature. For the first part of the table containing the branching fractions, we apply the following modified procedure. Since the tree-dominated modes are dominated by amplitudes proportional to V_{ub} , there is a large normalization uncertainty from $|V_{ub}|^2$, which we do *not* include in the table. Instead, we calculate the theoretical uncertainty of the quantity $\text{BrAv}(\bar{B} \rightarrow f)/|V_{ub}|^2$.⁷ The error from $|V_{ub}|$ can easily be restored by assuming that $\text{BrAv}(\bar{B} \rightarrow f) \propto |V_{ub}|^2$. In the same way, one can also rescale the branching fractions to account for a value of $|V_{ub}/V_{cb}|$ different from 0.09. We handle the dependence on the heavy-to-light form factors in a similar way. In this case one notes that the colour-suppressed final states $\pi^0\pi^0$, $\pi^0\rho^0$, $\rho^0\rho^0$ are almost independent of the form factors, since they are dominated by spectator scattering. The other modes, however, are nearly proportional to the square of the form factor. To remove the trivial dependence on the form factor uncertainty, which might be reducible in the future, we calculate the theoretical uncertainty of the quantity $\text{BrAv}(\bar{B} \rightarrow f)/f_+^{B\pi}(0)^2$ for the modes marked in the table with (\star), of $\text{BrAv}(\bar{B} \rightarrow f)/A_0^{B\rho}(0)^2$ for those marked with ($\star\star$), and of $\text{BrAv}(\bar{B} \rightarrow f)/(f_+^{B\pi}(0)A_0^{B\rho}(0))$ for the mode $\bar{B} \rightarrow \pi^\pm\rho^\mp$ marked with (\dagger). Once again, the full form-factor error can be restored by assuming the dependence on the form factor as divided out above, and the branching fractions can be approximately rescaled to other form-factor values by multiplying the appropriate factor.

Scanning the numbers in the “Theory I” column of Table 3, we notice that the R_{+-} and R_{00} ratios are systematically below the data, while the absolute branching fractions for the colour-allowed modes with only charged particles in the final state are consistently above. A plausible interpretation of this trend is that λ_B is in fact smaller than the default value $\lambda_B = 350$ MeV (a smaller value enhancing the colour-suppressed amplitude), and that the heavy-to-light form factors are about 10% smaller than the QCD sum rule central values that we assumed in Table 1 and used for “Theory I”.⁸ Since we have already seen in Section 6.3.2 that a large value of λ_B is in conflict with data, we adopt the “small λ_B and form-factor hypothesis” and recalculate the theoretical prediction with the modified parameter values and ranges $f_+^{B\pi}(0) = 0.23 \pm 0.03$, $A_0^{B\rho}(0) = 0.28 \pm 0.03$, $\lambda_B(1 \text{ GeV}) = (0.20_{-0.00}^{+0.05})$ GeV. The result is column “Theory II” in Table 3. We consider these as our reference predictions to be tested against future more accurate experimental results.

Comparing now “Theory II” with measurements, we find good agreement for the branching fractions, except for $\pi^0\pi^0$ as already discussed. However, the theoretical uncertainty is also large for this mode. The same feature is reflected in the ratios, where $R_{00}^{\pi\pi}$ stands out as too small. The ratios R_C^π , R_C^ρ of colour-suppressed modes do not fit very well either, reflecting the fact that factorization likes to have $[\rho^0\rho^0]_L$ to be larger and $\pi^0\pi^0$ to be smaller than data. Nevertheless, uncertainties taken face value, there is no disagreement. The $\pi\rho$ ratios R_{1-6} are in good agreement with data, though the central value of R_5 shifts away from the data in scenario “Theory II”. Since R_4 and R_5 provide

⁷BrAv denotes the CP-averaged branching fraction.

⁸Alternatively, a smaller value of $|V_{ub}|$ might be considered. Indeed, our central values imply $|V_{ub}|f_+^{B\pi}(0) = 9.34 \cdot 10^{-4}$, which is slightly larger than (60).

access to the real part of $\alpha_2(\pi\rho)$ and $\alpha_2(\rho\pi)$, respectively [5], precise measurements of the $\pi\rho$ final states should provide further insight into the mechanism that generates the colour-suppressed tree amplitude.

7 Conclusion

We computed the two-loop vertex corrections to the colour-allowed and colour-suppressed tree amplitude in QCD factorization, completing the calculation of these amplitudes at NNLO. Technically, the calculation amounts to a matching calculation from QCD to SCET, involving two-loop renormalization and infrared subtractions of evanescent operators, and massive two-loop vertex integrals that depend on one dimensionless parameter, and the charm quark mass in some cases. We obtain fully analytic expressions for both amplitudes after integration over the Gegenbauer expansion, including the exact dependence on the charm quark mass. The massless result is in complete agreement with a recent independent calculation [13], as well as the charm mass dependence of the imaginary part [12], while the charm mass dependence of the real part agrees numerically.

The NNLO vertex correction to the colour-suppressed tree amplitude is sizable, ranging from 10% to 25% for the real and imaginary part, respectively, and is a few percent for the colour-allowed amplitude. When combined with the $\mathcal{O}(\alpha_s^2)$ correction to spectator scattering, already known from [6–8], we find a large cancellation, both in the real and imaginary parts, so that the overall NNLO correction to the topological tree amplitudes is small. This is somewhat unfortunate, since an enhancement rather than a cancellation in the colour-suppressed tree amplitude might have helped to cure the large discrepancy with experimental data in the $\pi^0\pi^0$ channel.

A dedicated phenomenological analysis of tree-dominated B decays to (quasi) two-body final states with pions and rho mesons shows that the QCD factorization approach obtains strong support from the factorization test performed in Section 6.3.1. Overall, the data is described very well within theoretical and experimental uncertainties, especially for low values of $\lambda_B \simeq 200$ MeV and smaller form factors. The most problematic observables remain those related to the $\pi^0\pi^0$ branching fraction, which is predicted too low. Since the combined NNLO correction is rather small, the generic features of factorization are unchanged compared to the NLO analysis of [5]. Numerical differences arise primarily from modified parameter choices. Our final results are the columns labelled “Theory II” contained in Tables 2 and 3.

Acknowledgement

We would like to thank Bernd Jantzen for useful discussions, and Oleg Tarasov for collaboration at an early stage of this work. This work is supported in part by the DFG Sonderforschungsbereich/Transregio 9 “Computergestützte Theoretische Teilchenphysik”. X.-Q. Li acknowledges support from the Alexander-von-Humboldt Stiftung. T.H. acknowledges support from the German Federal Ministry of Education and Re-

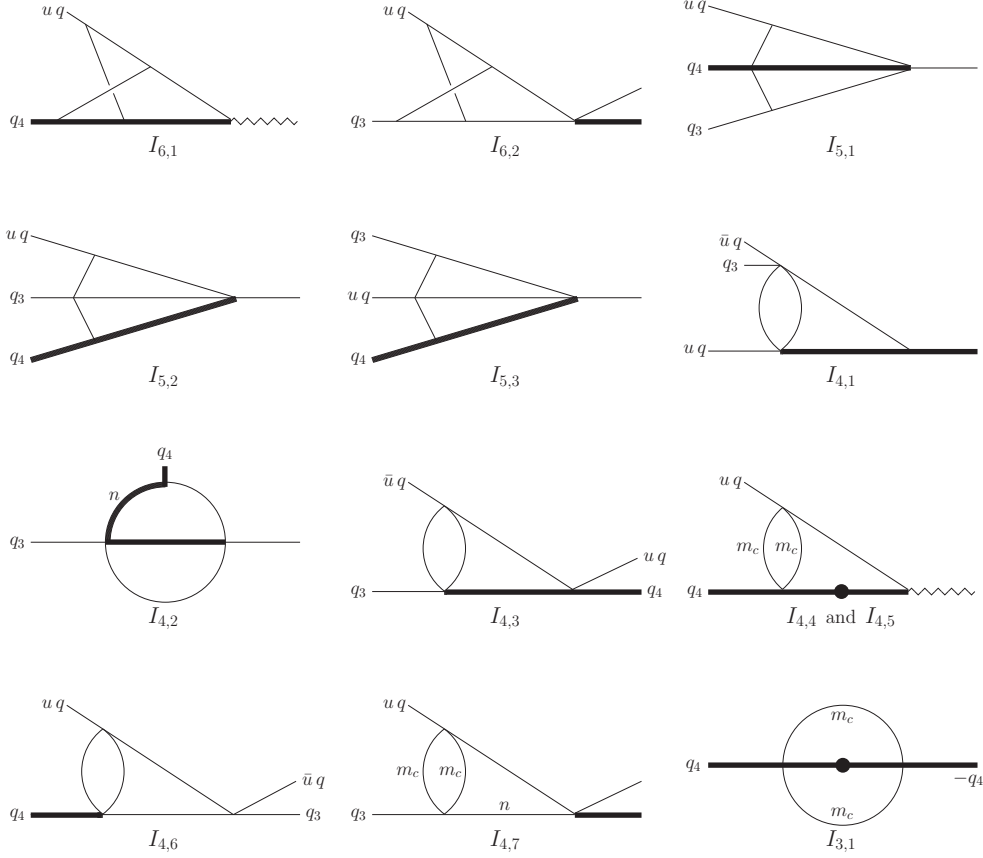


Figure 7: Selected master integrals. All momenta indicated are assumed to be incoming. Bold lines denote lines of mass m_b , and thin lines are massless unless otherwise indicated. Zig-zag lines have virtuality $\bar{u}m_b^2$. Dots on lines denote squared propagators, and the diagrams in question stand for both the undotted and the dotted integral. n represents a generalized propagator power.

search (BMBF). M.B. and T.H. acknowledge hospitality from the CERN theory group, where part of this work was performed.

A Master integrals

In this Appendix we list a few master integrals on which our results add to the ones given in [11], for instance by giving closed forms valid to all orders in $\epsilon = (4 - D)/2$. They are depicted in Figure 7. The expansions in ϵ are conveniently done with the package HypExp [36,37] and agree with the results given in [11]. Our notation for the integration measure is

$$\int [dk] \equiv \int \frac{d^D k}{(2\pi)^D}, \quad (68)$$

and we define the prefactor

$$S_\Gamma \equiv \frac{1}{(4\pi)^{D/2} \Gamma(1-\epsilon)} . \quad (69)$$

All momenta are incoming, and the kinematics is such that $q+q_3+q_4 = 0$ with $q^2 = q_3^2 = 0$ and $q_4^2 = m_b^2$. We tacitly assume that all propagators in the integrals below contain an infinitesimal $+i\eta$. We then have

$$\begin{aligned} I_{5,1} &= \int [dk_1] \int [dk_2] \frac{1}{[(k_1 + k_2 + q_4)^2 - m_b^2] (k_1 - uq)^2 (k_2 - q_3)^2 k_1^2 k_2^2} \\ &= -S_\Gamma^2 (m_b^2)^{-1-2\epsilon} \frac{\Gamma^2(1-\epsilon)\Gamma(1+2\epsilon)\Gamma(2+\epsilon)\Gamma^2(-\epsilon)}{\Gamma(2-\epsilon)} \\ &\quad \times \left\{ \frac{1-u}{u} {}_4F_3(1, 1, 1+2\epsilon, 2+\epsilon; 2, 2, 2-\epsilon; 1-u) \right. \\ &\quad \left. - \frac{1}{u} {}_4F_3(1, 1, 1+2\epsilon, 2+\epsilon; 2, 2, 2-\epsilon; 1) \right\} . \quad (70) \end{aligned}$$

$$\begin{aligned} I_{5,2} &= \int [dk_1] \int [dk_2] \frac{1}{[(k_2 - q_4)^2 - m_b^2] (k_1 + k_2 + q_3)^2 (k_1 - uq)^2 k_1^2 k_2^2} \\ &= -S_\Gamma^2 (m_b^2)^{-1-2\epsilon} \Gamma^2(1-\epsilon)\Gamma(-\epsilon)\Gamma(1+\epsilon) \\ &\quad \times \left\{ -u^{-3\epsilon} \Gamma(3\epsilon-1)\Gamma(-\epsilon) e^{3\pi i\epsilon} {}_2F_1(1-3\epsilon, 1-2\epsilon; 2-3\epsilon; u) \right. \\ &\quad \left. + u^{-2\epsilon} \frac{\Gamma(1-\epsilon)\Gamma(2\epsilon-1)\Gamma(-\epsilon)}{\Gamma(1-3\epsilon)\Gamma(1+\epsilon)} e^{2\pi i\epsilon} {}_3F_2(1, 1-2\epsilon, 1-\epsilon; 2-2\epsilon, 1+\epsilon; u) \right. \\ &\quad \left. - \frac{\Gamma(2\epsilon)}{3\epsilon} {}_3F_2(1, 1, 1+\epsilon; 2, 1+3\epsilon; u) \right\} . \quad (71) \end{aligned}$$

For the next integral it is convenient to split up the integration over y into the three sub-intervals $0 \dots u/(u+1) \dots u \dots 1$. Alternatively, one can compute this master integral by using the method of differential equations.

$$\begin{aligned} I_{5,3} &= \int [dk_1] \int [dk_2] \frac{1}{[(k_2 - q_4)^2 - m_b^2] (k_1 + k_2 + uq)^2 (k_1 - q_3)^2 k_1^2 k_2^2} \\ &= S_\Gamma^2 (m_b^2)^{-1-2\epsilon} \frac{\Gamma^2(1-\epsilon)\Gamma(1+2\epsilon)\Gamma(1+\epsilon)\Gamma(-\epsilon)}{2\epsilon^2} \int_0^1 dy \frac{y^{-4\epsilon}}{u-y} \\ &\quad \times \left[{}_2F_1(\epsilon, 2\epsilon; 1-\epsilon; \frac{\bar{y}(u+i\eta-y)}{y^2}) - {}_2F_1(\epsilon, 2\epsilon; 1-\epsilon; \frac{(y-u+i\eta)}{y}) \right] \\ &= -S_\Gamma^2 (m_b^2)^{-1-2\epsilon} \left\{ \frac{1}{\epsilon} \left[-\frac{1}{6} \ln^3(u) + \frac{1}{2} \ln(1-u) \ln^2(u) - \frac{1}{6} \pi^2 \ln(u) + \text{Li}_3(1-u) \right] \right\} \end{aligned}$$

$$\begin{aligned}
& +\text{Li}_3(u) + i\pi \left(\frac{1}{2} \ln^2(u) + \text{Li}_2(1-u) + \frac{\pi^2}{6} \right) \Big] \\
& + \frac{3 \ln^4(u)}{8} - \frac{5}{6} \ln(1-u) \ln^3(u) - 4 \ln^2(1-u) \ln^2(u) + \frac{5}{2} \text{Li}_2(u) \ln^2(u) - \frac{1}{3} \pi^2 \ln^2(u) \\
& + \frac{19}{6} \pi^2 \ln(1-u) \ln(u) - 5 \ln(1-u) \text{Li}_2(u) \ln(u) - 11 \text{Li}_3(1-u) \ln(u) - \frac{5}{2} \text{Li}_2^2(u) \\
& - 11 \text{Li}_3(u) \ln(u) + \text{Li}_4(1-u) + 13 \text{Li}_4(u) - 6 S_{2,2}(u) + 6 \ln(1-u) \zeta(3) - \frac{209 \pi^4}{360} \\
& + \frac{13}{6} \pi^2 \text{Li}_2(u) - 6 \ln(1-u) \text{Li}_3(u) + i\pi \left(\frac{5}{2} \ln(1-u) \ln^2(u) - \text{Li}_2(u) \ln(u) \right. \\
& \left. - \frac{5}{3} \pi^2 \ln(u) + 2 \text{Li}_3(1-u) + 7 \text{Li}_3(u) - \frac{3}{2} \ln^3(u) \right) + \mathcal{O}(\epsilon) \Big\} . \tag{72}
\end{aligned}$$

$$\begin{aligned}
I_{4,1} &= \int [dk_1] \int [dk_2] \frac{1}{[(k_1 - uq)^2 - m_b^2] (k_1 + q_3 + \bar{u}q)^2 (k_1 + k_2)^2 k_2^2} \\
&= -S_\Gamma^2 (m_b^2)^{-2\epsilon} \frac{\Gamma^5(1-\epsilon)}{\Gamma(2-2\epsilon)} \\
&\quad \times \left\{ -\bar{u}^{1-3\epsilon} \frac{\Gamma(3\epsilon-1)\Gamma(1-2\epsilon)}{\Gamma(2-2\epsilon)} e^{3\pi i \epsilon} {}_2F_1(1-\epsilon, 1-2\epsilon; 2-2\epsilon; u) \right. \\
&\quad \left. + \frac{\Gamma(1-3\epsilon)\Gamma(3\epsilon)}{\Gamma^2(1-\epsilon)\Gamma(2-3\epsilon)} G_{33}^{23} \left(\bar{u} \left| \begin{array}{l} \{0, 1-\epsilon, 1-2\epsilon\}, \{\} \\ \{0, 1-2\epsilon\}, \{1-3\epsilon\} \end{array} \right. \right) \right\} . \tag{73}
\end{aligned}$$

The Meijer-G functions can be written as a linear combination of hypergeometric functions [97]. The latter are then expanded in ϵ with **HypExp**. The next integral is a master only for $n = 1$ but for convenience we generalize one of the propagator powers.

$$\begin{aligned}
I_{4,2} &= \int [dk_1] \int [dk_2] \frac{1}{[(k_2 + q_4)^2 - m_b^2]^n [(k_1 + k_2 + q_4)^2 - m_b^2] (k_1 - q_3)^2 k_2^2} \\
&= S_\Gamma^2 (-1)^{-n} (m_b^2)^{1-n-2\epsilon} \frac{\Gamma^2(1-\epsilon)}{\Gamma(n)} G_{44}^{24} \left(1 \left| \begin{array}{l} \{1-\epsilon-n, 1-n, \epsilon, 2-n-2\epsilon\}, \{\} \\ \{0, 1-\epsilon-n\}, \{-n, \epsilon-1\} \end{array} \right. \right) . \tag{74}
\end{aligned}$$

$$\begin{aligned}
I_{4,3} &= \int [dk_1] \int [dk_2] \frac{1}{[(k_2 + q_4)^2 - m_b^2] k_1^2 (k_1 + k_2 - q)^2 (k_2 - uq)^2} \\
&= -S_\Gamma^2 (m_b^2)^{-2\epsilon} \frac{\Gamma^4(1-\epsilon)\Gamma(\epsilon)\Gamma(2\epsilon)\Gamma(1-2\epsilon)}{\Gamma(2-2\epsilon)\Gamma(2-\epsilon)} {}_2F_1(1, 2\epsilon; 2-\epsilon; \bar{u}) . \tag{75}
\end{aligned}$$

$$I_{4,4} = \int [dk_1] \int [dk_2] \frac{1}{[(k_1 + q_4)^2 - m_b^2] (k_1 - uq)^2 [k_2^2 - m_c^2] [(k_1 + k_2)^2 - m_c^2]}$$

$$\begin{aligned}
&= -S_\Gamma^2 (m_b^2)^{-2\epsilon} \left\{ \frac{1}{2\epsilon^2} + \frac{1}{\epsilon} \left(\frac{5}{2} - \frac{u \ln(u)}{u-1} \right) + \frac{2u \text{Li}_2(1-u)}{u-1} + \frac{2u \ln^2(u)}{u-1} \right. \\
&\quad \left. - \frac{5u \ln(u)}{u-1} + \frac{\pi^2}{2} + \frac{19}{2} + f_{44}(z, 1-u) + \mathcal{O}(\epsilon) \right\}, \tag{76}
\end{aligned}$$

with

$$\begin{aligned}
f_{44}(z, x) &\equiv - \int_{c_1-i\infty}^{c_1+i\infty} \frac{dw_1}{2\pi i} \int_{c_2-i\infty}^{c_2+i\infty} \frac{dw_2}{2\pi i} \\
&\quad \times \frac{2^{2w_1-1} \pi^{5/2} (1-x)^{w_2} z^{w_1} \csc(\pi w_1) \csc(\pi w_2) \Gamma(-2w_1 - w_2 + 1) \Gamma(w_1 + w_2)}{(w_1 - 1) w_1 \Gamma\left(\frac{3}{2} - w_1\right)} \tag{77}
\end{aligned}$$

and $z = m_c^2/m_b^2$. The two-fold Mellin-Barnes integration is along straight lines parallel to the imaginary axis, hence the real parts along the curves are constant. They read, respectively, $c_1 = 2/3$ and $c_2 = -1/2$. The form (76) of $I_{4,4}$ enables us to obtain fully analytic results for the amplitudes α_1 and α_2 , since we can interchange the integration over u with the Mellin-Barnes integrations.

$$\begin{aligned}
I_{4,5} &= \int [dk_1] \int [dk_2] \frac{1}{[(k_1 + q_4)^2 - m_b^2]^2 (k_1 - uq)^2 [k_2^2 - m_c^2] [(k_1 + k_2)^2 - m_c^2]} \\
&= -S_\Gamma^2 (m_b^2)^{-1-2\epsilon} \left\{ -\frac{1}{\epsilon} \frac{\ln(u)}{u-1} + \frac{\ln(u) \ln(zu)}{u-1} + \frac{\text{Li}_2(1-u)}{u-1} + f_{45}(z, 1-u) + \mathcal{O}(\epsilon) \right\}, \tag{78}
\end{aligned}$$

with

$$\begin{aligned}
f_{45}(z, x) &\equiv - \int_{c_1-i\infty}^{c_1+i\infty} \frac{dw_1}{2\pi i} \int_{c_2-i\infty}^{c_2+i\infty} \frac{dw_2}{2\pi i} \\
&\quad \times \frac{2^{2w_1-1} \pi^{5/2} (1-x)^{w_2} z^{w_1} \csc(\pi w_1) \csc(\pi w_2) \Gamma(-2w_1 - w_2) \Gamma(w_1 + w_2 + 1)}{w_1 \Gamma\left(\frac{3}{2} - w_1\right)} \tag{79}
\end{aligned}$$

and $c_1 = -1/24$ and $c_2 = -5/6$.

$$\begin{aligned}
I_{4,6} &= \int [dk_1] \int [dk_2] \frac{1}{k_1^2 (k_1 + k_2 + q)^2 (k_2 - q_3)^2 (k_2 + \bar{u}q)^2} \\
&= -S_\Gamma^2 (m_b^2)^{-2\epsilon} \frac{\Gamma^5(1-\epsilon) \Gamma(\epsilon) \Gamma(2\epsilon) \Gamma(1-2\epsilon)}{\Gamma(2-2\epsilon) \Gamma(2-3\epsilon) \Gamma(1+\epsilon)} e^{2\pi i \epsilon} {}_2F_1(1, 2\epsilon; 1+\epsilon; u). \tag{80}
\end{aligned}$$

In the next integral we again generalize one of the propagator powers.

$$\begin{aligned}
I_{4,7} &= \int [dk_1] \int [dk_2] \frac{1}{[(k_1 + q_3)^2]^n (k_1 - uq)^2 [k_2^2 - m_c^2] [(k_1 + k_2)^2 - m_c^2]} \\
&= S_\Gamma^2 (-1)^{-n} (m_c^2)^{1-n-2\epsilon} \frac{\Gamma^2(1-\epsilon)}{\Gamma(n)} \sqrt{\pi} 2^{1-2n-2\epsilon} \\
&\quad \times G_{44}^{24} \left(-\frac{u}{4z} - i\eta \left| \begin{array}{l} \{1-\epsilon-n, 1-n, 0, 2-n-2\epsilon\}, \{\} \\ \{0, 1-\epsilon-n\}, \{\frac{1}{2}-n-\epsilon, \epsilon-1\} \end{array} \right. \right). \tag{81}
\end{aligned}$$

The remaining integrals from Figure 7 can be found in the literature and shall not be given explicitly here: The integral $I_{6,1}$ through order $\mathcal{O}(\epsilon^0)$ can be found in [98], whereas an all-order result for $I_{6,2}$ is contained in [99]. The three-line master integral $I_{3,1}$ can be found in various papers [100–103].

B Auxiliary functions

B.1 Hard-scattering kernels

In this Appendix we list the explicit expressions for the right-insertion hard-scattering kernels. The wrong-insertion kernels can be obtained from linear combinations of the right-insertion ones, see (36). The one-loop hard-scattering kernels in the CMM operator basis read

$$\begin{aligned}
T_1^{(1)} &= \frac{C_F}{2N_c} \left(-6L + \ln^2(1-u) + 2\ln(u)\ln(1-u) - \frac{2\ln(1-u)}{u} \right. \\
&\quad \left. + 3\ln(1-u) - \ln^2(u) + \frac{\ln(u)}{u-1} + 3\ln(u) + 4\text{Li}_2(u) - \frac{\pi^2}{3} - 22 \right. \\
&\quad \left. + i\pi \left[2\ln(1-u) - 2\ln(u) - 3 \right] \right), \\
T_2^{(1)} &= 0, \tag{82}
\end{aligned}$$

with

$$L \equiv \ln \left(\frac{\mu^2}{m_b^2} \right). \tag{83}$$

At two loops, the kernels are conveniently subdivided into the following building blocks

$$\begin{aligned}
T_1^{(2)} &= T_1^{(2),re} + i\pi T_1^{(2),im} + n_l T_f (T_{1,n_l}^{(2),re} + i\pi T_{1,n_l}^{(2),im}) \\
&\quad + T_f (T_{1,T_f}^{(2),re} + i\pi T_{1,T_f}^{(2),im}) + T_f (T_{1,c}^{(2),re} + i\pi T_{1,c}^{(2),im}), \\
T_2^{(2)} &= T_2^{(2),re} + i\pi T_2^{(2),im}. \tag{84}
\end{aligned}$$

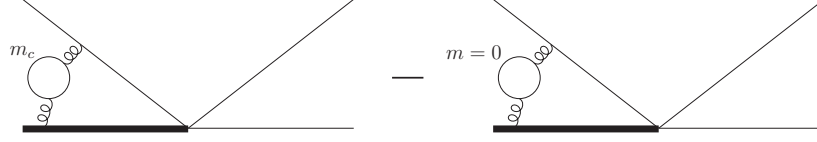


Figure 8: Diagrammatic representation of the charm-mass dependent term. Three further diagram differences are not shown.

The charm-quark contribution $T_f (T_{1,c}^{(2),re} + i\pi T_{1,c}^{(2),im})$ to $T_1^{(2)}$ arises from charm-loop insertions into the gluon propagator of the non-factorizable one-loop diagrams. It is designed such as to give the difference between the contribution of a quark of mass m_c and a massless quark, see Figure 8. This construction ensures that we set $n_l = 4$ irrespective of whether we treat the charm quark as massive or massless. The explicit expressions for the two-loop hard-scattering kernels are

$$\begin{aligned}
T_1^{(2),re} = & \frac{(47u^5 - 278u^4 + 1223u^3 - 2316u^2 + 2036u - 652) \ln^4(1-u)}{162(u-1)^2u^3} \\
& - \frac{(2u^3 + 4u^2 + 173u + 16) \ln^3(1-u)}{81u} - \frac{(4u^3 - 61u^2 - 436u + 16) \ln^2(1-u)}{54u^2} \\
& + \frac{2(73u^5 + 38u^4 - 1103u^3 + 2316u^2 - 2036u + 652) \ln(u) \ln^3(1-u)}{81(u-1)^2u^3} \\
& - \frac{(17u^3 + 300u^2 - 1098u + 978) \ln^2(u) \ln^2(1-u)}{27u^3} \\
& - \frac{\pi^2(9u^5 + 166u^4 - 1167u^3 + 2316u^2 - 2036u + 652) \ln^2(1-u)}{81(u-1)^2u^3} \\
& + \frac{(2u^5 - 20u^3 + 125u^2 - 76u - 52) \ln(u) \ln^2(1-u)}{27(u-1)^2u} + \frac{2}{9} \ln^3(u) \ln(1-u) \\
& + \frac{7(u-2)^2 \ln(2-u) \ln^2(1-u)}{9(u-1)^2} + \frac{16}{9} \text{Li}_2(u) \ln^2(1-u) \\
& + \frac{(2u^6 + 4u^5 - 191u^4 - 167u^3 + 1022u^2 - 646u - 6) \ln^2(u) \ln(1-u)}{27(u-1)u^3} \\
& - \frac{\pi^2(2u^5 + 355u^3 - 623u^2 + 385u - 140) \ln(1-u)}{81(u-1)^2u} \\
& - \frac{(4u^4 - 638u^3 + 1487u^2 - 1597u + 664) \ln(u) \ln(1-u)}{27(u-1)u^2}
\end{aligned}$$

$$\begin{aligned}
& + \frac{14(u-2)^2 \text{Li}_2(u-1) \ln(1-u)}{9(u-1)^2} + \frac{16(6u^2 - 16u - 5) \text{Li}_3(u) \ln(1-u)}{27(u-1)^2} \\
& - \frac{2(94u^3 - 271u^2 + 166u + 32) \text{Li}_2(u) \ln(1-u)}{27(u-1)^2 u} + \frac{(1601u - 1172) \ln(1-u)}{54u} \\
& + \frac{4(4u^3 - 50u^2 + 183u - 163) \ln(u) \text{Li}_2(u) \ln(1-u)}{27u^3} \\
& + \frac{(2u^3 - 436u^2 + 657u - 332) \ln^2(u)}{27(u-1)u} - \frac{8(3u^2 - 14u - 19) \zeta(3) \ln(1-u)}{27(u-1)^2} \\
& + \frac{2(20u^5 - 94u^4 + 292u^3 - 579u^2 + 509u - 163) \text{Li}_2(u)^2}{27(u-1)^2 u^3} \\
& + \frac{\pi^2(4u^4 - 435u^3 + 3174u^2 - 5346u + 2688)}{162(u-1)u^2} + \frac{64}{9} \text{Li}_3(1-u) \ln(1-u) \\
& - \frac{\pi^4(225u^5 + 378u^4 - 5914u^3 + 11598u^2 - 10198u + 3266)}{2430(u-1)^2 u^3} \\
& + \frac{16(u^3 + 2u - 2) \text{HPL}(\{-2, 2\}, 1-u)}{27u^3} - \frac{(2u^3 + 4u^2 - 313u + 273) \ln^3(u)}{81(u-1)} \\
& - \frac{8(u-2)(5u^2 - 6u + 2) \text{HPL}(\{-1, 2\}, 1-u)}{27(u-1)u^2} - \frac{47 \ln^4(u)}{162} \\
& + \frac{\pi^2(u-2)(53u^3 - 104u^2 - 16u + 4) \ln(2-u)}{81(u-1)^2 u^2} - \frac{65}{81} \pi^2 \ln^2(u) \\
& - \frac{\pi^2(2u^5 + 4u^4 - 427u^3 + 1209u^2 - 2140u + 1320) \ln(u)}{81(u-1)u^2} \\
& + \frac{(1601u - 942) \ln(u)}{54(u-1)} - \frac{4(u^2 - 3) \ln(u) \text{Li}_2(-u)}{27u^3} - \frac{4\pi^2(u^3 + 2u - 2) \text{Li}_2(u-1)}{81u^3} \\
& + \frac{2\pi^2(33u^3 + 400u^2 - 1472u + 1312) \ln(1-u) \ln(u)}{81u^3} - \frac{16}{27} \text{HPL}(\{-2, 2\}, u) \\
& + \frac{2\pi^2(2u^4 + u^3 + 5u^2 + 9u - 9) \ln(u+1)}{81(u-1)u^3} + \frac{16(u+1)^2 \text{HPL}(\{-1, 2\}, u)}{27(u-1)u} \\
& - \frac{(8u^4 - 937u^3 + 1523u^2 - 1509u + 664) \text{Li}_2(u)}{27(u-1)u^2} - \frac{2(u^2 - 3) \ln^2(u) \ln(u+1)}{27u^3} \\
& - \frac{2\pi^2(10u^5 - 208u^4 + 1183u^3 - 2340u^2 + 2060u - 660) \text{Li}_2(u)}{81(u-1)^2 u^3} \\
& - \frac{2(34u^4 + 530u^3 - 1551u^2 + 972u + 6) \ln(u) \text{Li}_2(u)}{27(u-1)u^3} + \frac{4}{81} \pi^2 \text{Li}_2(-u)
\end{aligned}$$

$$\begin{aligned}
& + \frac{2(4u^7 + 2u^6 - 39u^5 - 63u^4 + 678u^3 - 959u^2 + 362u - 6) \operatorname{Li}_3(1-u)}{27(u-1)^2 u^3} \\
& - \frac{16(6u^3 + 50u^2 - 183u + 163) \ln(u) \operatorname{Li}_3(1-u)}{27u^3} + \frac{68}{27} \ln^2(u) \operatorname{Li}_2(u) \\
& - \frac{14(u-2)^2 \operatorname{Li}_3(u-1)}{9(u-1)^2} + \frac{4(u^2-3) \operatorname{Li}_3(-u)}{27u^3} - \frac{104}{9} \ln(u) \operatorname{Li}_3(u) \\
& + \frac{2(4u^7 + 2u^6 - 39u^5 + 743u^4 - 2747u^3 + 3350u^2 - 1292u - 6) \operatorname{Li}_3(u)}{27(u-1)^2 u^3} \\
& - \frac{4(86u^5 - 406u^4 + 1553u^3 - 2919u^2 + 2569u - 823) \operatorname{Li}_4(1-u)}{27(u-1)^2 u^3} \\
& + \frac{4(96u^5 - 372u^4 + 1283u^3 - 2316u^2 + 2036u - 652) \operatorname{Li}_4(u)}{27(u-1)^2 u^3} \\
& - \frac{16(5u^5 + 36u^4 - 289u^3 + 579u^2 - 509u + 163) \operatorname{Li}_4\left(\frac{u}{u-1}\right)}{27(u-1)^2 u^3} \\
& + \frac{2(62u^5 - 397u^4 + 1012u^3 - 1112u^2 + 428u + 2) \zeta(3)}{9(u-1)^2 u^3} \\
& + \frac{8(3u^3 + 100u^2 - 366u + 326) \ln(u) \zeta(3)}{27u^3} - \frac{16\pi^2(2u-1) \ln(2)}{27(u-1)u} - \frac{3793}{36} \\
& + L \left(-\frac{32}{81} \ln^3(1-u) + \frac{2(27u+4) \ln^2(1-u)}{27u} - \frac{32}{27} \ln(u) \ln^2(1-u) \right. \\
& - \frac{32}{27} \ln^2(u) \ln(1-u) + \frac{2(13u-10) \ln(1-u)}{3u} + \frac{4(51u-4) \ln(u) \ln(1-u)}{27u} \\
& - \frac{64}{27} \operatorname{Li}_2(u) \ln(1-u) + \frac{32}{81} \pi^2 \ln(1-u) + \frac{32 \ln^3(u)}{81} - \frac{2(51u-43) \ln^2(u)}{27(u-1)} \\
& - \frac{2\pi^2(27u-23)}{81(u-1)} + \frac{26(3u-2) \ln(u)}{9(u-1)} + \frac{8(39u^2-39u+2) \operatorname{Li}_2(u)}{27(u-1)u} \\
& \left. - \frac{64}{27} \ln(u) \operatorname{Li}_2(u) - \frac{64}{27} \operatorname{Li}_3(1-u) + \frac{64 \operatorname{Li}_3(u)}{27} - 55 \right) - \frac{26L^2}{3}, \tag{85}
\end{aligned}$$

where the functions HPL denote the harmonic polylogarithms [43]. We proceed with

$$\begin{aligned}
T_1^{(2),im} &= \frac{8}{81} \ln^3(1-u) + \frac{2(u^3 + 2u^2 - 53u + 10) \ln^2(1-u)}{27u} + \frac{8}{9} \ln(u) \ln^2(1-u) \\
& + \frac{(4u^2 + 455u - 40) \ln(1-u)}{27u} + \frac{8}{27} \operatorname{Li}_2(u) \ln(1-u) - \frac{64}{81} \pi^2 \ln(1-u)
\end{aligned}$$

$$\begin{aligned}
& -\frac{2(2u^4 + 4u^3 - 40u^2 + 31u - 12) \ln(u) \ln(1-u)}{27(u-1)u} - \frac{56}{27} \ln^2(u) \ln(1-u) \\
& + \frac{2\pi^2(3u^3 + 5u^2 - 8u - 5)}{81(u-1)} + \frac{(2u^3 + 4u^2 + 38u - 57) \ln^2(u)}{27(u-1)} + \frac{4 \ln^3(u)}{27} \\
& - \frac{(4u^2 + 221u - 210) \ln(u)}{27(u-1)} + \frac{40}{81} \pi^2 \ln(u) - \frac{4}{27} u \text{Li}_2(u) - \frac{8}{3} \ln(u) \text{Li}_2(u) \\
& + \frac{20 \text{Li}_2(u)}{27(u-1)} - \frac{8 \text{Li}_2(u)}{27u} + \frac{4 \text{Li}_2(u)}{9} - \frac{80}{27} \text{Li}_3(1-u) + \frac{40 \text{Li}_3(u)}{9} - \frac{1609}{54} \\
& + L \left(-\frac{16}{27} \ln^2(1-u) - \frac{4(39u-35) \ln(u)}{27(u-1)} - \frac{64 \text{Li}_2(u)}{27} + \frac{16\pi^2}{81} \right. \\
& \left. + \frac{4(39u-4) \ln(1-u)}{27u} - \frac{32}{27} \ln(u) \ln(1-u) + \frac{16 \ln^2(u)}{27} - \frac{26}{3} \right), \quad (86)
\end{aligned}$$

$$\begin{aligned}
T_{1,n_i}^{(2),re} &= \frac{8}{27} \ln^3(1-u) - \frac{4(u+12) \ln^2(1-u)}{81u} - \frac{16}{27} \ln(u) \ln^2(1-u) \\
& + \frac{16}{27} \ln^2(u) \ln(1-u) - \frac{4(51u-32) \ln(1-u)}{81u} \\
& - \frac{8(19u-16) \ln(u) \ln(1-u)}{81(u-1)} + \frac{16}{27} \pi^2 \ln(1-u) + \frac{8(14u-11) \ln^2(u)}{81(u-1)} \\
& + \frac{4\pi^2(19u-16)}{243(u-1)} - \frac{4(51u-32) \ln(u)}{81(u-1)} - \frac{16}{27} \pi^2 \ln(u) - \frac{8 \ln^3(u)}{27} \\
& - \frac{8 \text{Li}_2(u)}{27(u-1)} - \frac{16 \text{Li}_2(u)}{27u} - \frac{232 \text{Li}_2(u)}{81} - \frac{16}{27} \text{Li}_3(1-u) + \frac{16 \text{Li}_3(u)}{27} + \frac{250}{27} \\
& + L \left(-\frac{8}{27} \ln^2(1-u) - \frac{8(3u-2) \ln(1-u)}{27u} - \frac{16}{27} \ln(u) \ln(1-u) \right. \\
& \left. + \frac{8 \ln^2(u)}{27} - \frac{8(3u-2) \ln(u)}{27(u-1)} - \frac{32 \text{Li}_2(u)}{27} + \frac{8\pi^2}{81} + \frac{136}{27} \right) + \frac{8L^2}{9}, \quad (87)
\end{aligned}$$

$$\begin{aligned}
T_{1,n_i}^{(2),im} &= \frac{8}{27} \ln^2(1-u) - \frac{152}{81} \ln(1-u) - \frac{8 \ln^2(u)}{27} + \frac{80 \ln(u)}{81} + \frac{68}{27} \\
& - \frac{8}{27} L \left(2 \ln(1-u) - 2 \ln(u) - 3 \right). \quad (88)
\end{aligned}$$

The terms arising from the bottom quark-loop insertion into the gluon line read:

$$T_{1,T_f}^{(2),re} = L \left(-\frac{8}{27} \ln^2(1-u) - \frac{8(3u-2) \ln(1-u)}{27u} - \frac{16}{27} \ln(u) \ln(1-u) \right)$$

$$\begin{aligned}
& + \frac{8 \ln^2(u)}{27} - \frac{8(3u-2) \ln(u)}{27(u-1)} - \frac{32 \text{Li}_2(u)}{27} + \frac{8\pi^2}{81} + \frac{136}{27} \Big) + \frac{8L^2}{9} \\
& - \frac{4(51u-32) \ln(1-u)}{81u} - \frac{8(19u-16) \ln(u) \ln(1-u)}{81(u-1)} - \frac{4(51u-32) \ln(u)}{81(u-1)} \\
& + \frac{16(47u-31) \ln(1-u)}{81(u-1)^2} + \frac{256}{81u^2} - \frac{760}{81u} + \frac{250}{27} \\
& + \frac{16(19u^3-39u^2+54u-16) \ln(u) \ln(1-u)}{81u^3} + \frac{56 \text{Li}_2(u)}{27(u-1)} \\
& - \frac{4\pi^2(19u^5-18u^4-75u^3+196u^2-126u+36)}{243(u-1)^3 u^2} + \frac{16(47u-16) \ln(u)}{81u^2} \\
& - \frac{224 \text{Li}_2(u)}{27u} + \frac{256 \text{Li}_2(u)}{81(u-1)^3} - \frac{256 \text{Li}_2(u)}{81u^3} + \frac{232 \text{Li}_2(u)}{81} + \frac{32 \text{Li}_2(u)}{3u^2} - \frac{16 \text{Li}_3(u)}{27} \\
& + \frac{16(u^3-6u+6) \text{Li}_3(1-u)}{27u^3} + \frac{32(3u^3-3u^2+3u-1) \zeta(3)}{9(u-1)^2 u^3} - \frac{1840}{81(u-1)} \\
& - \frac{256}{81(u-1)^2} - \frac{128 \ln^3(2)}{27(u-1)^2} + \frac{64\pi^2 \ln(2)}{27(u-1)^2} + \frac{4(6\omega_1-1)}{243\omega_1\sqrt{\omega_1}} p_1(\omega_1) \\
& + \frac{32}{81} p_2(\omega_1) - \frac{(15\phi_1+23)}{243\phi_1\sqrt{\phi_1}} p_1(\phi_1) - \frac{4(5\phi_1^2+6\phi_1-3)}{81\phi_1^2} p_2(\phi_1), \tag{89}
\end{aligned}$$

$$\begin{aligned}
T_{1,T_f}^{(2),im} &= -\frac{8}{27} L \left(2 \ln(1-u) - 2 \ln(u) - 3 \right) + \frac{68}{27} - \frac{880}{81(u-1)} + \frac{128}{81u} - \frac{64 \ln^2(2)}{9(u-1)^2} \\
& + \frac{32(6\omega_1-1)}{81\omega_1\sqrt{\omega_1}} p_3(\omega_1) - \frac{32}{27} p_4(\omega_1) - \frac{8(15\phi_1+23)}{81\phi_1\sqrt{\phi_1}} p_3(\phi_1) \\
& + \frac{4(5\phi_1^2+6\phi_1-3)}{27\phi_1^2} p_4(\phi_1), \tag{90}
\end{aligned}$$

with the abbreviations

$$\omega_1 \equiv \frac{\frac{u}{4}}{\frac{u}{4}+1}, \quad \phi_1 \equiv \frac{\frac{1-u}{4}}{\frac{1-u}{4}+1}, \tag{91}$$

and the auxiliary functions

$$\begin{aligned}
p_1(x) &= 12 \ln^2 \left(\frac{\sqrt{x}+1}{2\sqrt{1-x}} \right) - 3 \ln^2(1-x) + 12 \ln \left(\frac{2(\sqrt{x}+1)}{\sqrt{1-x}} \right) \ln(1-x) \\
& - 24 \ln \left(\frac{\sqrt{x}+1}{\sqrt{1-x}} \right) \ln(x) - 24 \text{Li}_2 \left(\frac{\sqrt{x}+1}{2} \right) - 24 \text{Li}_2(-\sqrt{x}) \\
& + 24 \text{Li}_2(\sqrt{x}) - 24 \ln^2(2) + 2\pi^2,
\end{aligned}$$

$$\begin{aligned}
p_2(x) &= 2 \ln^3 \left(\frac{\sqrt{x} + 1}{\sqrt{1-x}} \right) - \pi^2 \ln \left(\frac{2(\sqrt{x} + 1)}{\sqrt{1-x}} \right) - 3 \text{Li}_3 \left(\frac{1 - \sqrt{x}}{\sqrt{x} + 1} \right) + 2 \ln^3(2), \\
p_3(x) &= \ln \left(\frac{\sqrt{x} + 1}{\sqrt{1-x}} \right), \\
p_4(x) &= \ln \left(\frac{\sqrt{x} + 1}{2\sqrt{1-x}} \right) \ln \left(\frac{2(\sqrt{x} + 1)}{\sqrt{1-x}} \right). \tag{92}
\end{aligned}$$

The charm-mass dependent parts mentioned at the beginning of the section read

$$\begin{aligned}
T_{1,c}^{(2),re} &= -\frac{8}{27} \ln^3(1-u) + \frac{4(u+12) \ln^2(1-u)}{81u} + \frac{16}{27} \ln(u) \ln^2(1-u) - \frac{1840z}{81(u-1)} \\
&+ \frac{8}{27} \ln(z) \ln^2(1-u) + \frac{8(u-1)^2 \ln^2(1-u)}{27uz} - \frac{16}{27} \ln^2(u) \ln(1-u) - \frac{256z}{81(u-1)^2} \\
&- \frac{32(5u+3) \ln(1-u)}{81u} + \frac{880z \ln(1-u)}{81(u-1)} + \frac{8(19u-16) \ln(u) \ln(1-u)}{81(u-1)} - \frac{760z}{81u} \\
&+ \frac{16z \ln(u) \ln(1-u)}{9u} - \frac{8u^2 \ln(u) \ln(1-u)}{27(u-1)z} + \frac{8(3u-2) \ln(z) \ln(1-u)}{27u} + \frac{256z}{81u^2} \\
&+ \frac{16}{27} \ln(u) \ln(z) \ln(1-u) - \frac{8(u-1)^2 \ln(z) \ln(1-u)}{27uz} - \frac{16(u-1)^2 \ln(1-u)}{27uz} \\
&- \frac{16}{27} \pi^2 \ln(1-u) + \frac{8 \ln^3(u)}{27} - \frac{8\pi^2(u-2)z^2}{27u^2} - \frac{8(14u-11) \ln^2(u)}{81(u-1)} - \frac{4\pi^2(u+2)}{243(u-1)} \\
&- \frac{16z \ln^2(u)}{9u} + \frac{8u^2 \ln^2(u)}{27(u-1)z} - \frac{4(19u^3 - 42u^2 + 39u - 8)z \ln^2(z)}{81(u-1)^2u^2} - \frac{4 \ln^2(z)}{9} \\
&- \frac{4\pi^2(55u^3 - 132u^2 + 111u - 26)z}{243(u-1)^2u^2} - \frac{8(149u^3 - 192u^2 + 75u - 16)z \ln(z)}{81(u-1)^2u^2} \\
&+ \frac{16(19u-16) \ln(u)}{81(u-1)} + \frac{8(u-1)f_{44}(z,u)}{27z} + \frac{8(u^3 - 6z^2u + 6z^2)f_{44}(z,1-u)}{27u^2z} \\
&+ \frac{304z \ln(u)}{81u} + \frac{8(3u^2 - 2zu - 6u + 6z + 3)(u^2 + 4zu - 2u + 1)f_{45}(z,u)}{81(u-1)^2z} \\
&- \frac{8(3u^2 - 7zu + 4z)(u^2 - 4zu + 4z)f_{45}(z,1-u)}{81u^2z} - \frac{16u^2 \ln(u)}{27(u-1)z} + \frac{16}{27} \pi^2 \ln(u) \\
&- \frac{8}{27} \ln^2(u) \ln(z) + \frac{8(3u-2) \ln(u) \ln(z)}{27(u-1)} + \frac{16z \ln(u) \ln(z)}{9u} - \frac{8u^2 \ln(u) \ln(z)}{27(u-1)z} \\
&- \frac{8}{9} \ln(1-z) \ln(z) - \frac{8\pi^2}{81} \ln(z) + \frac{4(3u^2 - 3u + 1)(\pi^2u - 6\text{Li}_2(u))}{81(u-1)uz} + \frac{16z\text{Li}_2(u)}{9u}
\end{aligned}$$

$$\begin{aligned}
& + \frac{8(29u^2 - 20u - 6)\text{Li}_2(u)}{81(u-1)u} - \frac{8(u^3 + 12u^2 - 15u + 10)z\text{Li}_2(1-z)}{81(u-1)^2u^2} - \frac{8\text{Li}_2(z)}{9} \\
& + \frac{32}{27}\ln(z)\text{Li}_2(u) - \frac{8(2u-1)\text{Li}_2(1-z)}{27z} + \frac{4(u-2)z^2q_7(z)}{9u^2} + \frac{8(2u-1)q_8(z)}{27\sqrt{z}} \\
& - \frac{16(2u^3 - 21u^2 + 29u - 14)z^{3/2}q_8(z)}{81(u-1)^2u^2} - \frac{8(9u^2 - 5u - 2)\sqrt{z}q_8(z)}{81(u-1)u} + \frac{64z^2\zeta(3)}{9(u-1)^2} \\
& - \frac{128z^2\ln^3(2)}{27(u-1)^2} + \frac{64\pi^2z^2\ln(2)}{27(u-1)^2} + \frac{16}{27}\text{Li}_3(1-u) - \frac{16\text{Li}_3(u)}{27} + \frac{4(6\omega_z - 1)}{243\omega_z\sqrt{\omega_z}}p_1(\omega_z) \\
& + \frac{32}{81}p_2(\omega_z) - \frac{(15\phi_z + 23)}{243\phi_z\sqrt{\phi_z}}p_1(\phi_z) - \frac{4(5\phi_z^2 + 6\phi_z - 3)}{81\phi_z^2}p_2(\phi_z), \tag{93}
\end{aligned}$$

$$\begin{aligned}
T_{1,c}^{(2),im} &= -\frac{64\ln^2(2)z^2}{9(u-1)^2} - \frac{16(47u+8)z}{81(u-1)u} - \frac{8}{27}\ln^2(1-u) + \frac{8\ln^2(u)}{27} + \frac{16}{27}\ln(1-u)\ln(z) \\
& + \frac{152}{81}\ln(1-u) - \frac{80\ln(u)}{81} - \frac{16}{27}\ln(u)\ln(z) - \frac{8\ln(z)}{9} + \frac{32(6\omega_z - 1)}{81\omega_z\sqrt{\omega_z}}p_3(\omega_z) \\
& - \frac{32}{27}p_4(\omega_z) - \frac{8(15\phi_z + 23)}{81\phi_z\sqrt{\phi_z}}p_3(\phi_z) + \frac{4(5\phi_z^2 + 6\phi_z - 3)}{27\phi_z^2}p_4(\phi_z), \tag{94}
\end{aligned}$$

where now

$$\omega_z \equiv \frac{\frac{u}{4z}}{\frac{u}{4z} + 1}, \quad \phi_z \equiv \frac{\frac{1-u}{4z}}{\frac{1-u}{4z} + 1}, \tag{95}$$

as well as $z = m_c^2/m_b^2$. The other functions, notably f_{44} , f_{45} , q_7 , and q_8 , can be found in (77), (79), and (99), respectively. The two-loop expressions for the kernel $T_2^{(2)}$ related to the insertion of the operator Q_2 are simpler. They are

$$\begin{aligned}
T_2^{(2),re} &= \frac{4(u-4)(u^4 - 2u^3 + 7u^2 - 8u + 3)\ln^4(1-u)}{27(u-1)^2u^3} + \frac{32(2u+1)\text{Li}_3(u)\ln(1-u)}{9(u-1)^2} \\
& + \frac{2(u^3 + 2u^2 + 7u - 4)\ln^3(1-u)}{27u} + \frac{(2u^3 - 27u^2 - 12u + 8)\ln^2(1-u)}{9u^2} \\
& - \frac{16(2u^5 - 8u^4 + 16u^3 - 36u^2 + 35u - 12)\ln(u)\ln^3(1-u)}{27(u-1)^2u^3} + \frac{4\ln^4(u)}{27} \\
& + \frac{4(u^3 - 6u^2 + 33u - 36)\ln^2(u)\ln^2(1-u)}{9u^3} + \frac{2(u-2)^2\ln(2-u)\ln^2(1-u)}{3(u-1)^2} \\
& - \frac{8\pi^2(u^5 + 2u^4 - 13u^3 + 36u^2 - 35u + 12)\ln^2(1-u)}{27(u-1)^2u^3} - \frac{8}{9}\text{Li}_2(u)\ln^2(1-u)
\end{aligned}$$

$$\begin{aligned}
& - \frac{2(u^5 - 23u^3 + 87u^2 - 92u + 30) \ln(u) \ln^2(1-u)}{9(u-1)^2 u} - \frac{8}{27} \ln^3(u) \ln(1-u) \\
& - \frac{2(u^6 + 2u^5 - 5u^4 + 12u^3 - 63u^2 + 51u - 3) \ln^2(u) \ln(1-u)}{9(u-1)u^3} - \frac{4}{9} \pi^2 \ln^2(u) \\
& - \frac{(151u - 86) \ln(1-u)}{9u} + \frac{2\pi^2(u^5 - 8u^3 + 75u^2 - 95u + 30) \ln(1-u)}{27(u-1)^2 u} \\
& + \frac{32\pi^2(u^3 + 2u^2 - 11u + 12) \ln(u) \ln(1-u)}{27u^3} + \frac{4(u-2)^2 \text{Li}_2(u-1) \ln(1-u)}{3(u-1)^2} \\
& + \frac{2(2u^4 - 50u^3 + 14u^2 + 81u - 42) \ln(u) \ln(1-u)}{9(u-1)u^2} - \frac{16}{3} \text{Li}_3(1-u) \ln(1-u) \\
& + \frac{4(12u^3 - 53u^2 + 58u - 20) \text{Li}_2(u) \ln(1-u)}{9(u-1)^2 u} - \frac{32(2u+1)\zeta(3) \ln(1-u)}{9(u-1)^2} \\
& + \frac{8(4u^3 - 2u^2 + 11u - 12) \ln(u) \text{Li}_2(u) \ln(1-u)}{9u^3} + \frac{2(u^2 - 3) \ln^2(u) \ln(u+1)}{9u^3} \\
& + \frac{4(8u^5 - 16u^4 + 24u^3 - 36u^2 + 35u - 12) \text{Li}_2(u)^2}{9(u-1)^2 u^3} + \frac{2\pi^2(u^2 - 3) \ln(u+1)}{9u^3} \\
& - \frac{\pi^2(2u^4 + 3u^3 - 100u^2 + 298u - 168)}{27(u-1)u^2} - \frac{2(u^3 - 34u^2 + 7u + 21) \ln^2(u)}{9(u-1)u} \\
& - \frac{\pi^4(62u^5 + 2u^4 - 195u^3 + 720u^2 - 700u + 240)}{405(u-1)^2 u^3} + \frac{4(u^2 - 3) \ln(u) \text{Li}_2(-u)}{9u^3} \\
& + \frac{2\pi^2(u-2)^2 \ln(2-u)}{3(u-1)^2} - \frac{(151u - 102) \ln(u)}{9(u-1)} + \frac{2(u-2)(u^2 + 4u - 3) \ln^3(u)}{27(u-1)} \\
& + \frac{2\pi^2(u^5 + 2u^4 - 23u^3 - 15u^2 + 136u - 96) \ln(u)}{27(u-1)u^2} - \frac{4(u-2)^2 \text{Li}_3(u-1)}{3(u-1)^2} \\
& - \frac{4\pi^2(4u^5 - 22u^4 + 61u^3 - 144u^2 + 140u - 48) \text{Li}_2(u)}{27(u-1)^2 u^3} \\
& + \frac{4(6u^4 - 26u^3 + 97u^2 - 75u + 3) \ln(u) \text{Li}_2(u)}{9(u-1)u^3} + \frac{8}{9} \ln^2(u) \text{Li}_2(u) \\
& - \frac{4(2u^7 + u^6 - 18u^5 + 79u^4 - 111u^3 + 63u^2 - 10u - 3) \text{Li}_3(1-u)}{9(u-1)^2 u^3} \\
& - \frac{32(u-4)(2u-3) \ln(u) \text{Li}_3(1-u)}{9u^3} + \frac{2(4u^4 - 97u^3 + 51u^2 + 83u - 42) \text{Li}_2(u)}{9(u-1)u^2}
\end{aligned}$$

$$\begin{aligned}
& -\frac{4(2u^7 + u^6 - 12u^5 - 12u^4 + 139u^3 - 220u^2 + 102u - 3) \text{Li}_3(u)}{9(u-1)^2u^3} \\
& -\frac{16}{3} \ln(u) \text{Li}_3(u) + \frac{8(2u^5 + 14u^4 - 69u^3 + 180u^2 - 175u + 60) \text{Li}_4(1-u)}{9(u-1)^2u^3} \\
& + \frac{8(2u^5 - 22u^4 + 57u^3 - 144u^2 + 140u - 48) \text{Li}_4(u)}{9(u-1)^2u^3} + \frac{1507}{18} \\
& -\frac{32(4u^4 - 14u^3 + 36u^2 - 35u + 12) \text{Li}_4\left(\frac{u}{u-1}\right)}{9(u-1)^2u^3} + \frac{32(u-4)(2u-3) \ln(u) \zeta(3)}{9u^3} \\
& -\frac{4(36u^5 - 86u^4 - 67u^3 + 227u^2 - 110u + 3) \zeta(3)}{9(u-1)^2u^3} - \frac{4(u^2 - 3) \text{Li}_3(-u)}{9u^3} \\
& + L \left(-\frac{4}{3} \ln^2(1-u) - \frac{4(3u-2) \ln(1-u)}{3u} - \frac{8}{3} \ln(u) \ln(1-u) \right. \\
& \left. + \frac{4 \ln^2(u)}{3} - \frac{4(3u-2) \ln(u)}{3(u-1)} - \frac{16 \text{Li}_2(u)}{3} + \frac{4\pi^2}{9} + 34 \right) + 4L^2, \tag{96}
\end{aligned}$$

$$\begin{aligned}
T_2^{(2),im} &= \frac{8}{27} \ln^3(1-u) - \frac{2(u^3 + 2u^2 - 5u + 6) \ln^2(1-u)}{9u} + \frac{16}{9} \ln(u) \ln^2(1-u) \\
& - \frac{4(u^2 + 29u - 5) \ln(1-u)}{9u} + \frac{4(u^4 + 2u^3 - 5u^2 + 6u - 2) \ln(u) \ln(1-u)}{9(u-1)u} \\
& + \frac{32}{9} \text{Li}_2(u) \ln(1-u) - \frac{8}{9} \pi^2 \ln(1-u) - \frac{16}{9} \ln^2(u) \ln(1-u) \\
& + \frac{8 \ln^3(u)}{27} - \frac{2(u^3 + 2u^2 + u - 1) \ln^2(u)}{9(u-1)} - \frac{2\pi^2(3u^3 + 5u^2 - 11u + 4)}{27(u-1)} \\
& + \frac{4}{9}(u+21) \ln(u) - \frac{8}{27} \pi^2 \ln(u) + \frac{4}{9} u \text{Li}_2(u) - \frac{32}{9} \ln(u) \text{Li}_2(u) + \frac{4 \text{Li}_2(u)}{9(u-1)} \\
& - \frac{8 \text{Li}_2(u)}{9u} - \frac{4 \text{Li}_2(u)}{3} + \frac{16}{9} \text{Li}_3(1-u) + \frac{16 \text{Li}_3(u)}{9} + \frac{155}{9} \\
& + L \left(-\frac{8}{3} \ln(1-u) + \frac{8 \ln(u)}{3} + 4 \right). \tag{97}
\end{aligned}$$

B.2 Charming functions

In this Appendix we list the expressions for the functions that depend on m_c . We define $z = m_c^2/m_b^2$ and

$$\eta \equiv \frac{4z}{(\sqrt{4z+1} + 1)^2},$$

$$\kappa \equiv 1 + \sqrt{z} . \quad (98)$$

In terms of these variables our building blocks read

$$\begin{aligned}
q_1(z) &= \ln^3(\eta) + 6 \ln(\eta) \text{Li}_2(\eta) - 6 \text{Li}_3(\eta) + 6\zeta(3) , \\
q_2(z) &= \ln(\eta) \sqrt{4z+1} , \\
q_3(z) &= 9 \ln^4(\eta) - 12\pi^2 \ln^2(\eta) + 144 \text{Li}_2^2(\eta) - 48\pi^2 \text{Li}_2(\eta) + 4\pi^4 , \\
q_4(z) &= \ln^3(\eta) - 2\pi^2 \ln(\eta) + 12 \text{Li}_3(\eta) - 12\zeta(3) , \\
q_5(z) &= -\ln^3(\eta) - 4 \ln^2(\eta) \text{Li}_2(\eta) + 2\pi^2 \ln(\eta) - 12 \text{Li}_3(\eta) + 12\zeta(3) , \\
q_6(z) &= [-3 \ln^2(\eta) - 12 \text{Li}_2(\eta) + 2\pi^2] \sqrt{4z+1} , \\
q_7(z) &= \ln^2(z) + 2 \text{Li}_2(1-z) + \pi^2 , \\
q_8(z) &= 2 \ln(\kappa) \ln(z) - \ln(1-z) \ln(z) - 4 \text{Li}_2(\sqrt{z}) + \text{Li}_2(z) + \pi^2 , \\
q_9(z) &= \text{Li}_3(1-z) - 2 \text{Li}_3(1-\sqrt{z}) - 2 \text{Li}_3(\sqrt{z}) + \text{Li}_3(z) + 2 \text{Li}_3\left(\frac{\sqrt{z}}{\sqrt{z}+1}\right) - 2\zeta(3) , \\
q_{10}(z) &= -\ln^3(z) + 3 \ln(1-z) \ln^2(z) + 6 \ln^2(\kappa) \ln(z) - 4\pi^2 \ln(z) - 4 \ln^3(\kappa) \\
&\quad + 8\pi^2 \ln(\kappa) + 12 q_9(z) , \\
q_{11}(z) &= \ln^4(z) + 24 \ln^2(\kappa) \ln^2(z) - 48 \ln(1-z) \ln(\kappa) \ln^2(z) + 8\pi^2 \ln^2(z) \\
&\quad + 12 \text{Li}_2(z) \ln^2(z) - 8\pi^2 \ln(1-z) \ln(z) + 16\pi^2 \ln(\kappa) \ln(z) + 16 \ln^3(\kappa) \ln(z) \\
&\quad - 96 \ln(1-\sqrt{z}) \ln(z) \text{Li}_2(-\sqrt{z}) - 192 \text{Li}_2(-\sqrt{z}) \text{Li}_2(\sqrt{z}) + 40\pi^2 \text{Li}_2(z) \\
&\quad - 96 \ln(\kappa) \ln(z) \text{Li}_2(\sqrt{z}) - 96\pi^2 \text{Li}_2(\sqrt{z}) + 8\pi^4 - 48 \ln(z) q_9(z) , \\
q_{12}(z) &= -4 \ln^3(1-z) + 6 \ln(z) \ln^2(1-z) + 12 \ln(2\kappa) \ln^2(1-z) + 3 \ln^2(z) \ln(1-z) \\
&\quad - 12 \ln^2(2\kappa) \ln(1-z) - 24 \ln(z) \ln(\kappa) \ln(1-z) - 4\pi^2 \ln(1-z) + 4 \ln^3(\kappa) \\
&\quad + 18 \ln^2(\kappa) \ln(z) - 12 \ln^2(2) \ln(z) + 8\pi^2 \ln(8z/\kappa) - 6 \ln(\kappa) \ln^2(z) \\
&\quad + 24 \ln(2) \ln(2z) \ln(\kappa) - 12 \ln(z) \text{Li}_2(z) - 24 \ln(z) \text{Li}_2\left(\frac{\kappa}{2}\right) - 24 \text{Li}_3\left(\frac{1-\sqrt{z}}{2}\right) \\
&\quad + 24 \text{Li}_3\left(\frac{2\sqrt{z}}{\sqrt{z}-1}\right) - 24 \text{Li}_3\left(\frac{2\sqrt{z}}{\sqrt{z}+1}\right) + 24 \text{Li}_3\left(\frac{\sqrt{z}}{\sqrt{z}+1}\right) + 24 \text{Li}_3\left(\frac{\kappa}{2}\right) \\
&\quad + 24 \text{Li}_3(1-\sqrt{z}) - 72 \text{Li}_3(\sqrt{z}) + 48 \ln(z) \text{Li}_2(\sqrt{z}) + 12 \text{Li}_3(z) - 24\zeta(3) . \quad (99)
\end{aligned}$$

References

- [1] M. Beneke, G. Buchalla, M. Neubert and C. T. Sachrajda, Phys. Rev. Lett. **83**, 1914 (1999) [hep-ph/9905312].
- [2] M. Beneke, G. Buchalla, M. Neubert and C. T. Sachrajda, Nucl. Phys. B **591**, 313 (2000) [hep-ph/0006124].
- [3] M. Beneke, G. Buchalla, M. Neubert and C. T. Sachrajda, Nucl. Phys. B **606**, 245 (2001) [hep-ph/0104110].
- [4] M. Beneke, G. Buchalla, M. Neubert and C. T. Sachrajda, Phys. Rev. D **72**, 098501 (2005) [hep-ph/0411171].
- [5] M. Beneke and M. Neubert, Nucl. Phys. B **675**, 333 (2003) [hep-ph/0308039].
- [6] M. Beneke and S. Jäger, Nucl. Phys. B **751** (2006) 160 [hep-ph/0512351].
- [7] V. Pilipp, Nucl. Phys. B **794** (2008) 154 [arXiv:0709.3214 [hep-ph]].
- [8] N. Kivel, JHEP **0705** (2007) 019 [hep-ph/0608291].
- [9] M. Beneke and S. Jäger, Nucl. Phys. B **768** (2007) 51 [hep-ph/0610322].
- [10] A. Jain, I. Z. Rothstein and I. W. Stewart, 0706.3399 [hep-ph].
- [11] G. Bell, arXiv:0705.3133v2 [hep-ph].
- [12] G. Bell, Nucl. Phys. B **795** (2008) 1 [arXiv:0705.3127 [hep-ph]].
- [13] G. Bell, Nucl. Phys. B **822** (2009) 172 [arXiv:0902.1915 [hep-ph]].
- [14] G. Bell, M. Beneke, T. Huber and Xin-Qiang Li, in progress.
- [15] G. Bell and V. Pilipp, Phys. Rev. D **80** (2009) 054024 [arXiv:0907.1016 [hep-ph]].
- [16] G. Buchalla, A. J. Buras and M. E. Lautenbacher, Rev. Mod. Phys. **68** (1996) 1125 [hep-ph/9512380].
- [17] K. G. Chetyrkin, M. Misiak and M. Münz, Nucl. Phys. B **520** (1998) 279 [hep-ph/9711280].
- [18] C. W. Bauer, S. Fleming, D. Pirjol and I. W. Stewart, Phys. Rev. D **63** (2001) 114020 [hep-ph/0011336].
- [19] C. W. Bauer, D. Pirjol and I. W. Stewart, Phys. Rev. D **65** (2002) 054022 [hep-ph/0109045].
- [20] M. Beneke, A. P. Chapovsky, M. Diehl and T. Feldmann, Nucl. Phys. B **643** (2002) 431 [hep-ph/0206152].

- [21] M. Beneke and T. Feldmann, Phys. Lett. B **553** (2003) 267 [hep-ph/0211358].
- [22] J. Chay and C. Kim, Nucl. Phys. B **680** (2004) 302 [hep-ph/0301262].
- [23] J. Charles, A. Le Yaouanc, L. Oliver, O. Pene and J. C. Raynal, Phys. Rev. D **60** (1999) 014001 [hep-ph/9812358].
- [24] M. Beneke and T. Feldmann, Nucl. Phys. B **592** (2001) 3 [hep-ph/0008255].
- [25] M. Beneke, Y. Kiyo and D. s. Yang, Nucl. Phys. B **692** (2004) 232 [hep-ph/0402241].
- [26] R. Bonciani and A. Ferroglia, JHEP **0811** (2008) 065 [arXiv:0809.4687 [hep-ph]].
- [27] H. M. Asatrian, C. Greub and B. D. Pecjak, Phys. Rev. D **78** (2008) 114028 [arXiv:0810.0987 [hep-ph]].
- [28] M. Beneke, T. Huber and X. Q. Li, Nucl. Phys. B **811** (2009) 77 [arXiv:0810.1230 [hep-ph]].
- [29] G. Bell, Nucl. Phys. B **812** (2009) 264 [arXiv:0810.5695 [hep-ph]].
- [30] G. Passarino and M. J. G. Veltman, Nucl. Phys. B **160** (1979) 151.
- [31] S. Laporta and E. Remiddi, Phys. Lett. B **379** (1996) 283 [hep-ph/9602417].
- [32] S. Laporta, Int. J. Mod. Phys. A **15** (2000) 5087 [hep-ph/0102033].
- [33] F. V. Tkachov, Phys. Lett. B **100** (1981) 65.
- [34] K. G. Chetyrkin and F. V. Tkachov, Nucl. Phys. B **192** (1981) 159.
- [35] C. Anastasiou and A. Lazopoulos, JHEP **0407** (2004) 046 [hep-ph/0404258].
- [36] T. Huber and D. Maitre, Comput. Phys. Commun. **175** (2006) 122 [hep-ph/0507094].
- [37] T. Huber and D. Maitre, Comput. Phys. Commun. **178** (2008) 755 [arXiv:0708.2443 [hep-ph]].
- [38] J. Gluza, K. Kajda and T. Riemann, Comput. Phys. Commun. **177** (2007) 879 [arXiv:0704.2423 [hep-ph]].
- [39] M. Czakon, Comput. Phys. Commun. **175** (2006) 559 [hep-ph/0511200].
- [40] A. V. Kotikov, Phys. Lett. B **254** (1991) 158.
- [41] A. V. Kotikov, Phys. Lett. B **259** (1991) 314.
- [42] A. V. Kotikov, Phys. Lett. B **267** (1991) 123.

- [43] E. Remiddi and J. A. M. Vermaseren, *Int. J. Mod. Phys. A* **15** (2000) 725 [hep-ph/9905237].
- [44] P. Gambino, M. Gorbahn and U. Haisch, *Nucl. Phys. B* **673** (2003) 238 [hep-ph/0306079].
- [45] M. Gorbahn and U. Haisch, *Nucl. Phys. B* **713** (2005) 291 [hep-ph/0411071].
- [46] G. P. Lepage and S. J. Brodsky, *Phys. Rev. D* **22** (1980) 2157.
- [47] A. V. Efremov and A. V. Radyushkin, *Phys. Lett. B* **94** (1980) 245.
- [48] M. Beneke and D. Yang, *Nucl. Phys. B* **736** (2006) 34 [hep-ph/0508250].
- [49] M. Misiak and M. Münz, *Phys. Lett. B* **344** (1995) 308 [hep-ph/9409454].
- [50] K. G. Chetyrkin, M. Misiak and M. Münz, *Nucl. Phys. B* **518** (1998) 473 [hep-ph/9711266].
- [51] M. Beneke, J. Rohrer and D. Yang, *Nucl. Phys. B* **774** (2007) 64 [hep-ph/0612290].
- [52] E. Gamiz, C. T. H. Davies, G. P. Lepage, J. Shigemitsu and M. Wingate [HPQCD Collaboration], *Phys. Rev. D* **80** (2009) 014503 [arXiv:0902.1815 [hep-lat]].
- [53] C. Bernard *et al.*, *PoS LATTICE2008* (2008) 278 [arXiv:0904.1895 [hep-lat]].
- [54] P. Ball and R. Zwicky, *Phys. Rev. D* **71** (2005) 014029 [hep-ph/0412079].
- [55] P. Ball and G. W. Jones, *JHEP* **0703** (2007) 069 [hep-ph/0702100].
- [56] C. Bobeth, M. Misiak and J. Urban, *Nucl. Phys. B* **574** (2000) 291 [hep-ph/9910220].
- [57] M. Beneke, T. Feldmann and D. Seidel, *Nucl. Phys. B* **612** (2001) 25 [hep-ph/0106067].
- [58] J. D. Bjorken, *Nucl. Phys. Proc. Suppl.* **11** (1989) 325.
- [59] E. Barberio *et al.* [Heavy Flavor Averaging Group], arXiv:0808.1297 [hep-ex], and updates at <http://www.slac.stanford.edu/xorg/hfag>.
- [60] B. Aubert *et al.* [BABAR Collaboration], *Phys. Rev. D* **76** (2007) 091102 [arXiv:0707.2798 [hep-ex]].
- [61] K. Abe *et al.*, *Phys. Rev. Lett.* **99** (2007) 121601 [hep-ex/0609015].
- [62] A. Bornheim *et al.* [CLEO Collaboration], *Phys. Rev. D* **68** (2003) 052002 [Erratum-*ibid.* *D* **75** (2007) 119907] [hep-ex/0302026].
- [63] P. Ball, *Phys. Lett. B* **644** (2007) 38 [hep-ph/0611108].

- [64] T. Becher and R. J. Hill, Phys. Lett. B **633** (2006) 61 [hep-ph/0509090].
- [65] B. Aubert *et al.* [BABAR Collaboration], Phys. Rev. Lett. **98** (2007) 091801 [hep-ex/0612020].
- [66] D. Becirevic and A. B. Kaidalov, Phys. Lett. B **478** (2000) 417 [hep-ph/9904490].
- [67] P. Ball and R. Zwicky, Phys. Rev. D **71** (2005) 014015 [hep-ph/0406232].
- [68] C. Albertus *et al.*, Phys. Rev. D **72** (2005) 033002 [hep-ph/0506048]; J. M. Flynn and J. Nieves, Phys. Rev. D **75** (2007) 013008 [hep-ph/0607258].
- [69] C. G. Boyd, B. Grinstein and R. F. Lebed, Phys. Rev. Lett. **74** (1995) 4603 [hep-ph/9412324]; C. G. Boyd and M. J. Savage, Phys. Rev. D **56** (1997) 303 [hep-ph/9702300].
- [70] P. Ball and E. Kou, JHEP **0304** (2003) 029 [hep-ph/0301135].
- [71] V. M. Braun, D. Y. Ivanov and G. P. Korchemsky, Phys. Rev. D **69** (2004) 034014 [hep-ph/0309330].
- [72] H. Kawamura and K. Tanaka, Phys. Lett. B **673** (2009) 201 [arXiv:0810.5628 [hep-ph]].
- [73] A. J. Buras, R. Fleischer, S. Recksiegel and F. Schwab, Phys. Rev. Lett. **92** (2004) 101804 [hep-ph/0312259]; A. J. Buras, R. Fleischer, S. Recksiegel and F. Schwab, Nucl. Phys. B **697** (2004) 133 [hep-ph/0402112].
- [74] B. Aubert *et al.* [BABAR Collaboration], Phys. Rev. D **75** (2007) 012008 [hep-ex/0608003].
- [75] M. Morello [CDF Collaboration], Nucl. Phys. Proc. Suppl. **170** (2007) 39 [hep-ex/0612018].
- [76] B. Aubert *et al.* [BABAR Collaboration], arXiv:0807.4226 [hep-ex].
- [77] K. Abe *et al.* [Belle Collaboration], arXiv:hep-ex/0610065.
- [78] B. Aubert *et al.* [BaBar Collaboration], Phys. Rev. Lett. **102** (2009) 141802 [arXiv:0901.3522 [hep-ex]].
- [79] J. Zhang *et al.* [BELLE Collaboration], Phys. Rev. Lett. **91** (2003) 221801 [hep-ex/0306007].
- [80] B. Aubert *et al.* [Babar Collaboration], Phys. Rev. D **76** (2007) 052007 [arXiv:0705.2157 [hep-ex]].
- [81] A. Somov *et al.*, Phys. Rev. Lett. **96** (2006) 171801 [hep-ex/0601024].

- [82] B. Aubert *et al.* [BaBar Collaboration], Phys. Rev. D **78** (2008) 071104 [arXiv:0807.4977 [hep-ex]].
- [83] C. C. Chiang *et al.* [Belle Collaboration], Phys. Rev. D **78** (2008) 111102 [arXiv:0808.2576 [hep-ex]].
- [84] R. Godang *et al.* [CLEO Collaboration], Phys. Rev. Lett. **88** (2002) 021802 [hep-ex/0101029].
- [85] B. Aubert *et al.* [BABAR Collaboration], Phys. Rev. Lett. **93** (2004) 051802 [hep-ex/0311049].
- [86] A. Kusaka *et al.* [Belle Collaboration], Phys. Rev. D **77** (2008) 072001 [arXiv:0710.4974 [hep-ex]].
- [87] C. P. Jessop *et al.* [CLEO Collaboration], Phys. Rev. Lett. **85** (2000) 2881 [hep-ex/0006008].
- [88] B. Aubert *et al.* [BABAR Collaboration], Phys. Rev. Lett. **91** (2003) 201802 [hep-ex/0306030].
- [89] H. n. Li and S. Mishima, arXiv:0901.1272 [hep-ph].
- [90] H. Y. Cheng and C. K. Chua, Phys. Rev. D **80** (2009) 074031 [arXiv:0908.3506 [hep-ph]].
- [91] B. Aubert *et al.* [BABAR Collaboration], Phys. Rev. D **76** (2007) 012004 [hep-ex/0703008].
- [92] A. Kusaka *et al.* [Belle Collaboration], Phys. Rev. Lett. **98** (2007) 221602 [hep-ex/0701015].
- [93] B. Aubert *et al.* [BABAR Collaboration], Phys. Rev. D **79** (2009) 072006 [arXiv:0902.2051 [hep-ex]].
- [94] A. Gordon *et al.* [Belle Collaboration], Phys. Lett. B **542** (2002) 183 [hep-ex/0207007].
- [95] B. Aubert *et al.* [BABAR Collaboration], Phys. Rev. D **75** (2007) 091103 [hep-ex/0701035].
- [96] J. Zhang *et al.* [BELLE Collaboration], Phys. Rev. Lett. **94** (2005) 031801 [hep-ex/0406006].
- [97] A. Erdélyi (ed.), Higher transcendental functions, Vol. 1, (McGraw-Hill, New York, 1953).
- [98] T. Huber, JHEP **0903** (2009) 024 [arXiv:0901.2133 [hep-ph]].

- [99] T. Gehrmann, T. Huber and D. Maitre, Phys. Lett. B **622** (2005) 295 [hep-ph/0507061].
- [100] F. A. Berends, A. I. Davydychev and N. I. Ussyukina, Phys. Lett. B **426** (1998) 95 [hep-ph/9712209].
- [101] M. Argeri, P. Mastrolia and E. Remiddi, Nucl. Phys. B **631** (2002) 388 [hep-ph/0202123].
- [102] T. Huber, Nucl. Phys. Proc. Suppl. **183**, 238 (2008) [arXiv:0807.0637 [hep-ph]].
- [103] S. Bekavac, A. G. Grozin, D. Seidel and V. A. Smirnov, Nucl. Phys. B **819** (2009) 183 [arXiv:0903.4760 [hep-ph]].